Scientific Research Publishing

Including Planet 9 in the Solar System Increases the Coherence between the Sunspot Number Record and Solar Inertial Motion

Ian Edmonds

Department of Physics, Queensland University of Technology, Brisbane, Australia
Email: iredmonds@aapt.net.au

Abstract

The Sun would be subject to a significant variation of orbital motion about the solar system barycentre if a small planet is orbiting at a very large distance. This paper assesses if the Planet 9 hypothesis, the existence of a ninth planet, is consistent with the planetary hypothesis: the synchronisation of sunspot emergence to solar inertial motion (SIM) induced by the planets. We show that SIM would be profoundly affected if Planet 9 exists and that the hypothesised effect of SIM on sunspot emergence would be radically different from the effect of SIM due to the existing eight planets. We compare the frequency and time variation of Sun to barycentre distance, R_B, calculated for both the eight and nine planet systems, with the frequency and time variation of sunspot number (SSN). We show that including Planet 9 improves the coherence between R_B and SSN in the decadal, centennial and millennial time range. Additionally, as the variation of R_B is sensitive to the longitude and period of Planet 9, it is possible to adjust both parameters to fit the variation of R_B to the SSN record and obtain new estimates of the period and present longitude of Planet 9. Finally, we develop the hypothesis that planetary induced solar acceleration reduces meridional flow and consequently sunspot emergence thereby providing an explanation for the observed coincidence of grand solar minima with intervals of extreme solar acceleration.

Keywords

Planet 9 Hypothesis, Planetary Hypothesis, Solar Inertial Motion, Reconstructed Sunspot Number, Phase Modulation of SSN, Future SSN Events

1. Introduction

The discovery of Neptune in 1846 was facilitated by observations suggesting the

orbit of Uranus was perturbed by an unknown planet. Subsequent calculations, based on the perturbations, provided an estimate of Neptune's location in the sky and shortly after it was observed directly. Recent astronomical observations of the orbits of several Kuiper Belt objects have led to the hypothesis that a ninth planet, far more distant than Neptune, exists and is perturbing the orbits [1]. Calculations, based on the apparent clustering of the longitude of perihelion of the objects, have provided estimates of the mass, semi major axis, eccentricity, and inclination of the hypothetical planet, known as Planet 9, and an indication that the current location of the planet is in the vicinity of Orion's Shield. Planet 9 has not been directly observed and the hypothesis that it exists is controversial. The absence of direct observation is due to the extreme difficulty of observing so distant a planet with existing telescopes. However, the controversy arises mainly from the fact that the hypothesis relies on the clustering in longitude of perihelion of just six objects out of a much larger population of objects and may be the result of selection bias [2]. Other than this clustering in longitude of perihelion of a few objects the additional supporting evidence appears to be limited to an apparent trend in the declination of Pluto over the past 20 years [3]. However, the trend favours a planet either more massive or closer than the planet hypothesised by [1] or possibly another planet, closer to Pluto, in addition to Planet 9; a result that tends to increase rather than decrease the controversy. Clearly, in the continuing absence of direct observation, e.g. [4]; other supporting evidence would be welcome.

A possible source of support for the Planet 9 hypothesis could come from the planetary hypothesis [5]; that there is a causal link between the cycles of sunspot number (SSN), such as the ~11 year Schwabe, ~88 year Gleissberg, ~1000 year Eddy and the ~2400 year Hallstatt cycles and planetary motion. The planetary hypothesis has been developed, with limited acceptance, e.g. [6]-[16]. The more conventional view of the origin of cycles in SSN is that sunspot emergence is irregular and is associated with the effect, on the solar dynamo, of random (stochastic) hydro-magnetic flows in the convective zone of the Sun [17] [18]. The origin of the cycles or quasi-cycles in sunspot emergence is controversial partly due to the extended range of sunspot cycle periodicity. Examples of longer term SSN cycles previously observed include cycles of ~60, ~88, ~104, ~150, ~208, and ~506 year period in the centennial periodicity range [9] [19], and the ~1000 year Eddy and ~2400 year Hallstaat cycles in the millennial periodicity range [13] [20] [21] [22]. Various theories have been proposed to account for this range of periodicity in sunspot emergence: some theories are based on purely interior mechanisms e.g. [23]-[29] and some theories are based on planetary synchronised mechanisms e.g. [9] [16] [30]. All previous planetary synchronism mechanisms have been based on the eight planet solar system. No study has investigated the possible effect of a distant ninth planet on planetary synchronised sunspot emergence.

The planetary synchronism of sunspot emergence due to the cyclic motion of Sun about the solar system barycentre, e.g. [6] [31] [32]; would be profoundly

affected, in terms of periodicity and time variation, by a ninth planet. The simple reason for this is that, as displacement of the Sun from the barycentre is proportional to the product of planet mass and planet distance from the barycentre, a very distant planet can have a large effect. Jose [6] calculated, for the years 1653 to 2060, the distance, R_B, between the Sun and the solar system barycentre for the eight planet system and was able to show a reasonable correlation between R_B and the record of SSN available at that time, up to 1964, provided the SSN was signed, *i.e.* each second cycle of SSN was given a negative sign. However, comparison of the timing of SIM with the occurrence of more recent decadal solar cycles proved unconvincing [7]. As a result subsequent studies of the connection between SIM and SSN shifted to comparisons of SIM with SSN on the centennial scale, specifically the occurrence of grand solar minima and maxima, e.g. [7] [15] [33]. With eight planets, relating SIM to SSN on the centennial and millennial scale has proven problematic due to R_B being essentially constant when averaged over centennial and millennial time scales [7] [34]; a fact confirmed in **Figure 1** of this paper. Nevertheless, workers have been able to find the ~2400 year cycle in the patterns of SIM [7] [35], in differences in the ordered and disordered states of SIM [14] [32] [33], and in very small variations in the average ellipticity of the solar orbit about the barycentre [13].
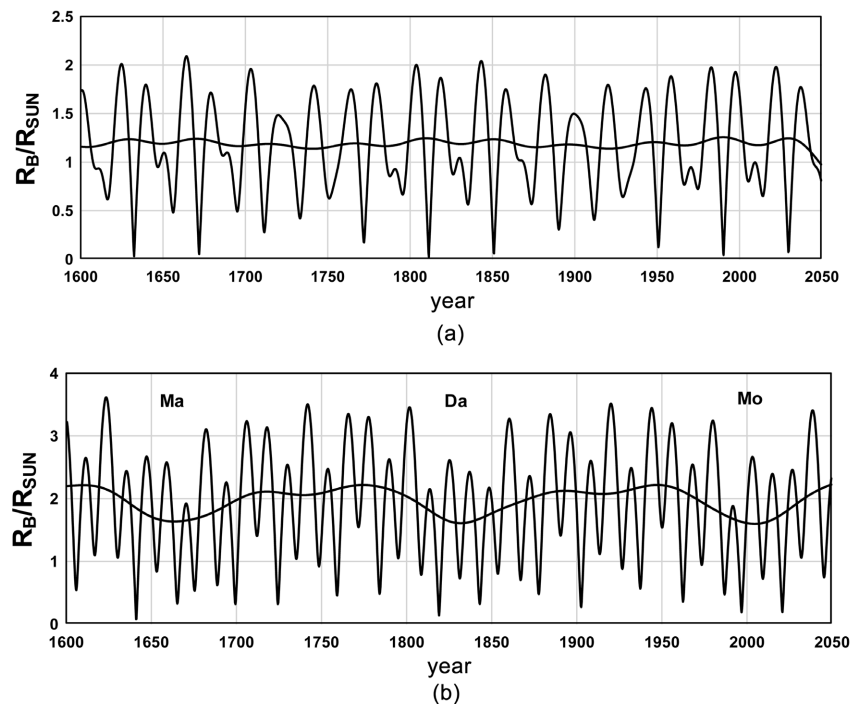

Figure 1. (a) R_B/R_{SUN} variation for $m_9 = 0$. (b) R_B/R_{SUN} variation for $m_9 = 7m_E$. The graphs illustrate the transition from predominantly bi-decadal periodicity when $m_9 = 0$, to a predominantly decadal periodicity when $m_9 = 7m_E$. Also shown are running averages over 35 years that indicate that large centennial time scale minima occur in R_B/R_{SUN} when $m_9 = 7m_E$ but insignificant centennial scale minima occur in R_B/R_{SUN} for the $m_9 = 0$, the eight planet system. Also indicated are the approximate times of occurrence of the Maunder, Dalton, and Modern grand minima in sunspot number.

In this paper we consider the possibility that relating SSN to SIM has proven difficult because the calculation of SIM has not included the effect of Planet 9. If Planet 9 exists, the projected mass, m_9, is about seven Earth masses, and the projected semi-major axis is about 380 AU [1]. The displacement of the Sun from the barycentre is proportional to the product $m_P r_P$ where m_P is the planet mass and r_P is the distance of the planet from the Sun. For Jupiter, $m_J = 318 m_E$ and r_J ~ 5.2 AU and for the hypothesised Planet 9, $m_9 \sim 7 m_E$, and $r_9 \sim 380$ AU. The ratio of the two displacements is $7 \times 380/318 \times 5.2 = 1.6$. So even though Planet 9 is very distant and orbiting very slowly, the displacement of the Sun by Planet 9 will be larger than the displacement due to Jupiter. Therefore, it is perhaps timely to consider if the inclusion of Planet 9 in calculations of SIM improves the frequency and time relationship of SIM to solar activity. The corollary, that if a nine planet formulation of SIM proves more consistent with the frequency and time dependence of solar activity than the current eight planet formulation, would in itself provide additional indirect evidence for the existence of Planet 9.

Section 2 of the paper briefly discusses the current knowledge of Planet 9 and outlines the data sources and the simplified method of calculating the time variation of the SIM used in the paper. Section 3 demonstrates that SIM with Planet 9 included provides a better fit to the decadal variation in SSN than SIM without Planet 9. Section 4 uses the observed SSN from 1610 to the present to show that recent grand solar minima in SSN are associated with large decreases in centennial scale averages of SIM. Section 5 demonstrates that, in the millennium scale variation of SIM with Planet 9 included, several significant components, the Hallstatt, Gleissberg, 60 and 30 year cycles, emerge and demonstrates that these components are absent in SIM without Planet 9. Additionally, it is shown that the low frequency spectral components of SIM are sensitive to the orbital period of Planet 9 and, consequently, the orbital period of Planet 9 can be tuned to fit the low frequency component of SIM to the Hallstatt cycle in solar activity. Section 6 shows that the problem of the Jose cycle in SIM being absent in SSN may be due to the phase modulation of the Jose cycle in the transformation from SIM to SSN. Section 7 introduces a mechanism for the influence of SIM on meridional flow in the convective region of the Sun and, ultimately, the influence of SIM on SSN. Section 8 is a conclusion.

2. Methods and Data Sources

2.1. Prior Evidence of Planet 9

Evidence for the existence of Planet 9 has been accumulating for about 20 years, [36] [37] [38] [39] [40]. Analysis of the evidence, the anomalous orbits of some Kuiper Belt objects, suggests the existence of a new planet of mass ~7 Earth masses, in an orbit of eccentricity ~0.3 with a semi major axis of ~380 AU inclined at ~15 degrees to the ecliptic plane [1]. However, the parameter estimates, based just on the anomalous clustering of a few distant objects, remain very uncertain [1].

2.2. Data Sources

Planet heliographic longitudes on January 01, 1965, were obtained from https://omniweb.gsfc.nasa.gov/coho/helios/heli.html. Group sunspot numbers 1610 to 2015 [41], were obtained from https://svalgaard.leif.org/research/gn-data.htm. Reconstructed SSN, −6755 to 1885, was obtained from https://www2.mps.mpg.de/projects/sun-climate/data/SN_composite.txt.

2.3. Method of Calculating SIM with Planet 9 Included

In view of the limited accuracy of the orbital parameters of Planet 9 SIM is calculated using a model where all the planets move about the Sun in circular orbits in the ecliptic plane. This is a good approximation for the known planets that have a significant effect on SIM, *i.e.* Jupiter, Saturn, Uranus and Neptune, as the orbits these planets are nearly circular and have low inclination to the ecliptic plane. As shown in Figure 1, the SIM, calculated using circular orbits for the eight known planets, is scarcely distinguishable from SIM calculated using exact planet orbits based on ephemeris data [6] [32] [34] [42]. However using a circular orbit for Planet 9 is an approximation as its orbit is projected to be eccentric, $\varepsilon \sim 0.3$, and inclined to the ecliptic, $i \sim 15°$ [1]. Including eccentricity and inclination of Planet 9 in the calculation of SIM would greatly increase the complexity of the calculation [42], and is outside the scope of this paper. Spectral analysis will be the major investigative tool in this paper and for basic spectral analysis like FFT equal time intervals are essential. With circular orbits, as used in this paper, equal time intervals occur naturally in the calculation of SIM whereas for eccentric orbits equal angular intervals occur naturally and the conversion to the equal time intervals required for FFT is complex. The orbital parameters of the planets used in the calculation are given in Table 1.

Table 1. Parameters of the planets.

Planet	Mass in mass Earth units, m_i	Radius, AU, r_i	Period, days T_i (years)	HGILong 01/01/1965, L_i
Jupiter	318	5.2	4332 (11.8)	340.2
Saturn	95	9.5	10,759 (29.4)	260.6
Venus	0.815	0.72	224.7 (0.615)	146.2
Earth	1	1	365.256 (1)	24.9
Neptune	17.15	30.07	60,195 (164.8)	152.6
Uranus	14.53	19.19	30,688 (84.0)	86.7
Mercury	0.055	0.387	87.969 (0.241)	85.2
Mars	0.107	1.524	687 (1.88)	63.8
Planet 9	7	380	2,700,000 (7400)	60 (fitted)
Sun	333,000			

The orbital period of Planet 9, $T_9 = 7400$ years, is obtained from the value of the semi-major axis, $a_9 = 380$ AU [1] and the use of Kepler's 3rd Law, $T^2/a^3 =$ constant. If T is measured in years and a is measured in AU, the constant = 1.

The time variation of the coordinates, (x_i, y_i), of the ith planet relative to the Sun as origin at (0,0) are calculated using

$$x_i = r_i \cos(\omega_i t + \varphi_i)$$
$$y_i = r_i \sin(\omega_i t + \varphi_i)$$
(1)

where r_i is the orbital radius of the ith planet, the angular frequency $\omega_i = 2\pi/T_i$, the phase angle in radians, $\phi_i = (\pi/180)L_i$, and L_i is the heliographic inertial longitude of the planet in degrees on January 01, 1965. The coordinates, (x_{PCM}, y_{PCM}), of the planetary centre of mass (PCM) relative to the Sun are given by

$$x_{PCM} = \sum m_i x_i / \sum m_i$$
$$y_{PCM} = \sum m_i y_i / \sum m_i$$
(2)

The distance between the Sun and the planetary centre of mass, r_{PCM}, is given by

$$r_{PCM} = \left(x_{PCM}^2 + y_{PCM}^2\right)^{1/2}$$
(3)

The distance between the Sun and the barycentre, R_B, is

$$R_B = r_{PCM}\left[\sum m_i / \left(\sum m_i + m_{SUN}\right)\right]$$
(4)

The Sun to barycentre distance is usually expressed as the ratio R_B/R_{SUN} where R_{SUN} is the radius of the Sun, 0.0046 AU.

3. Comparing the Decadal Variation of the SSN Record and R_B/R_{SUN}

3.1. The Decadal Scale Variation of R_B/R_{SUN}

Figure 1(a) shows the time variation of R_B/R_{SUN} for the eight planet system, $m_9 = 0$, and Figure 1(b) shows R_B/R_{SUN} for the nine planet system when $m_9 = 7m_E$. The most striking feature of Figure 1 is that the frequency of the cycles in R_B/R_{SUN} has doubled when $m_9 = 7m_E$. A second feature is that there is a significant centennial scale variation, ~170 year in period, when $m_9 = 7m_E$ that is not apparent when $m_9 = 0$.

Figure 2 compares the spectral content of the two variations of R_B/R_{SUN} in Figure 1. The spectrum of R_B/R_{SUN} for the eight planet system, $m_9 = 0$, is dominated by a component at period 19.5 years, with weaker components at 12.6 and 13.7 years and minor components at 35 and 46 years. Thus the periodicity of the eight planet variation is primarily bi-decadal. The periodicity of R_B/R_{SUN} for the nine planet system is dominated by the component at period 11.9 years with weaker components at 8.4, 13.7, 29.6, ~86 and ~172 years. Thus the periodicity of R_B/R_{SUN} for the nine planet system is primarily decadal. The component at 11.9 years is the synodic period of Jupiter with Planet 9. Similarly the components at 29.6 years, ~86 years and ~172 years are due to synodic periods with
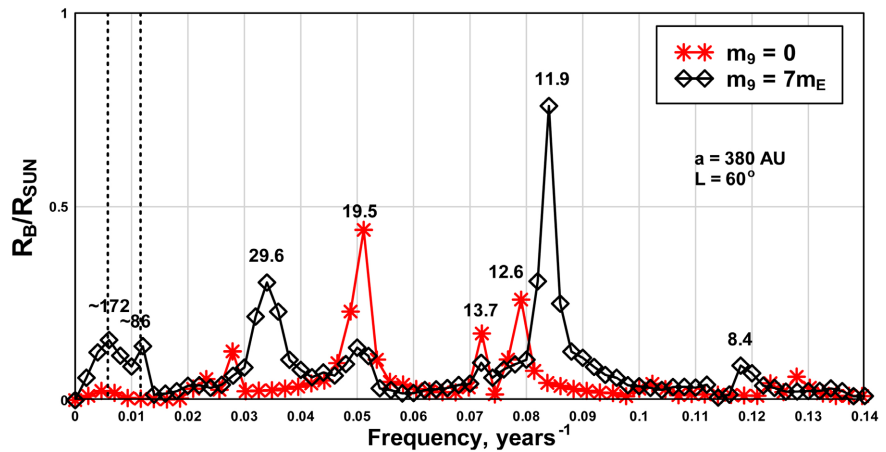
Figure 2. The spectral content of R_B/R_{SUN} for the eight planet solar system, (red stars), and R_B/R_{SUN} for the nine planet system (black diamonds). For the eight planet system progressively stronger peaks occur at 13.7, 12.6, and 19.5 years, with weak peaks at 36 and 45 years. When $m_9 = 7m_E$ significant peaks occur at ~172, ~86, 29.6, 11.9 and 8.4 years, with the dominant peak at 11.9 years.

Saturn, Uranus and Neptune respectively. The synodic period of a component is given by $T = 1/(1/T_P - 1/T_9)$.

A feature of R_B/R_{SUN} for the nine planet system is the presence of moderately strong components at ~86 years and ~172 years. The presence of these longer period components is also clearly evident in the time variation of **Figure 1(b)** where minima in the long term average value of R_B/R_{SUN} occur at ~170 year intervals with the minima separated by broad maxima. The pattern of broader maxima alternating with sharper minima is the result of the interference of the ~86 year and ~172 year cycles. That is, the deep centennial scale minima in **Figure 1(b)** occur when the two cycles are both in the negative part of their cycles. The labels Maunder, Dalton and Modern in **Figure 1(b)** correspond approximately to the central times of grand solar minima in SSN and the times clearly align with the centennial scale minima in R_B/R_{SUN}.

The transition from the primarily bi-decadal SIM for the eight planet system to a primarily decadal SIM for the nine planet system is quite dramatic so it is interesting to follow how this comes about. **Figure 3** compares the orbits of the Sun about the barycentre for the eight planet and the nine planet systems during the interval 1890 to 1913, centred on the year 1900, see **Figure 1(a)** and **Figure 1(b)**. In the left hand diagram of **Figure 3** the first minimum in R_B/R_{SUN} occurs at 1 followed by a maximum at 2 and another minimum at 3, with about 20 years between minima, *i.e.* ~bi-decadal periodicity. The right hand diagram shows the Sun orbit about the barycentre when $m_9 = 7m_E$ for two values of Planet 9 longitude, $L_9 = 60°$ and $L_9 = 240°$. The heliographic inertial longitude, L, is measured anticlockwise from the positive x axis.

For the $L_9 = 60°$ case there is a first minimum at 1, a first maximum at 2, a second minimum at 3, a second maximum at 4, and a third minimum at 5, with about 10 years between minima, *i.e.* ~decadal periodicity. The phase of the
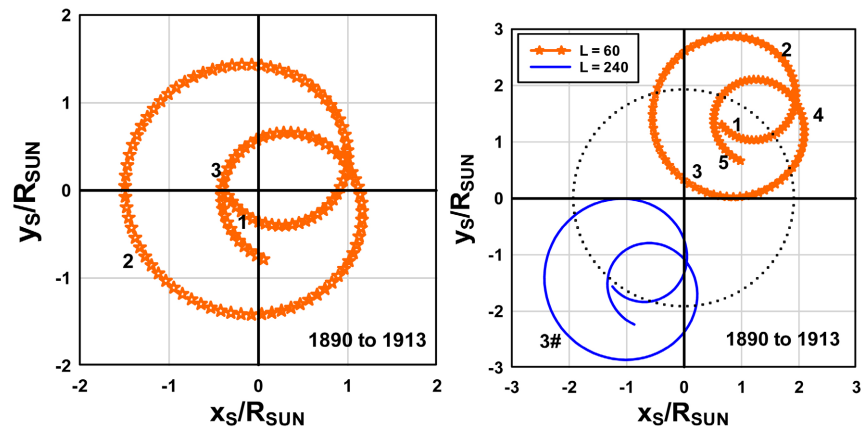
Figure 3. (LHS diagram): The anticlockwise motion of the Sun about the barycentre between 1890 and 1913 for the eight planet system. This time interval is centred on the year 1900 in **Figure 1(a)**. Three extremes in Sun to barycentre distance occur: 1, minimum; 2, maximum; and 3, minimum; corresponding to $a \sim 20$ year periodicity in Sun to barycentre distance, R_B. (RHS diagram): Orbits of the Sun for the nine planet system in the same time interval centred on year 1900 in **Figure 1(b)**. The Sun motion is shown for cases of Planet 9 longitudes, $L = 60°$ and $L = 240°$. Planet longitude is measured anticlockwise relative to the positive x axis. For the case where $L = 60°$ five extremes in Sun motion occur: 1, minimum; 2, maximum; 3, minimum; 4, maximum; and 5, minimum; corresponding to $a \sim 11$ year periodicity in Sun to barycentre distance, R_B. The dotted circle represents the approximate long term average value of R_B/R_{SUN} over the time interval of one circular orbit of Planet 9, period ~7000 years. Note that, in Section 5, we show that the long term average value of R_B/R_{SUN} actually varies by approximately 2.5%, from a maximum of 1.95 to a minimum of 1.90 with a period of ~2400 years, the Hallstatt cycle period.

~decadal cycle is sensitive to Planet 9 longitude. This is illustrated in **Figure 3** for the case of $L_9 = 240°$ where the orbital pattern due primarily to Jupiter, Saturn, Uranus, and Neptune has moved from the upper right hand quadrant to the lower left hand quadrant of the diagram. The minimum in R_B/R_{SUN} at 3 occurring at about 1901 is now a maximum in R_B/R_{SUN} at 3# occurring at about 1901. It is apparent that when the longitude of Planet 9 changes by 180° the phase of the short, ~decadal, cycle in R_B/R_{SUN} also changes by 180°.

3.2. Comparing the Decadal Variations of R_B/R_{SUN} and SSN

The group sunspot number (GSS) [41], extends from 1610 to 2015 (**Figure 4**). By removing the 20 year running average we obtain the primarily decadal variation of GSS. The GSS, before 1700, during the Maunder Minimum is of low accuracy [41], so here we use GSS in the interval between 1700 and 2015 to compare with the variation of R_B/R_{SUN} (**Figure 5**). In **Figure 5** we use the normalised variations, *i.e.* the variations divided by their standard deviation, to compare the GSS and R_B/R_{SUN}. There are 28 GSS cycles between 1705.5 and 2014.5. Thus, the average GSS period between the maximum at 1705.5 and the maximum at 2014.5 is 309/28 = 11.03 years. If the hypothesised forcing of SSN due to SIM occurs at the dominant periodicity of R_B/R_{SUN} in the decadal time range, *i.e.* at 11.9 years, see
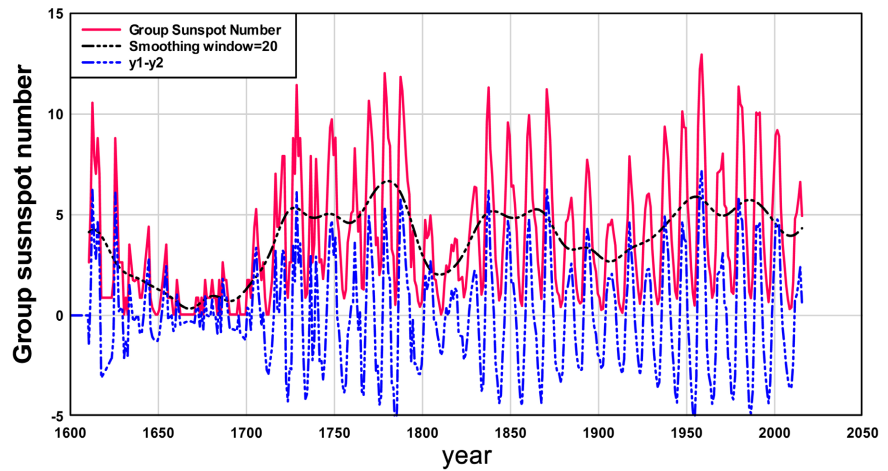
Figure 4. The group sunspot number (GSS) [41], (red curve) is reduced to the primarily decadal variation, (blue broken curve), by removing the long term variation. The estimated accuracy of the GSS prior to 1700 is low and is not used in the comparison of R_B/R_{SUN} with GSS in **Figure 5**.
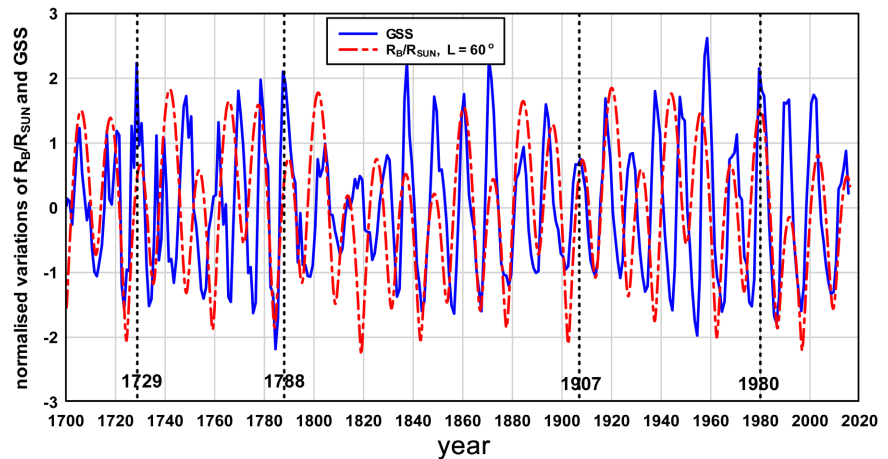

Figure 5. Compares the normalised variations of GSS and R_B/R_{SUN} for the nine planet system. The dotted reference lines mark the two interval ranges when the Schwabe cycle in the GSS jumps in phase by 360°, *i.e.* adds an additional cycle, relative to the R_B/R_{SUN} cycle.

Figure 2, we would expect 309/11.9 = 26 forcing cycles during this interval. That is, there are 28 GSS cycles compared with 26 SIM cycles during this 309 year long interval. As a result there are two 360° phase jumps apparent in **Figure 5**. The first occurs in the interval between 1729 and 1788, (at ~1758), and the second occurs between 1907 and 1980, (at ~1943). Stephani *et al.* [43] observed phase jumps in the Schwabe cycle at around the same times as observed here.

As is evident from **Figure 3**, the phase of the dominant decadal periodicity in R_B/R_{SUN} is strongly dependent on the longitude of Planet 9. For example, the minimum labelled 3 in **Figure 3** of the orbital pattern when $L_9 = 60°$ becomes a maximum, labelled 3#, in the orbital pattern when $L_9 = 240°$. If the correlation coefficient between GSS variation and the R_B/R_{SUN} variation is calculated as the

Planet 9 longitude is varied the correlation passes through a sharp maximum of 0.3 when $L_9 = 60°$ as shown in Figure 6. The moderately high correlation coefficient is a result of the fairly close correspondence of the dominant periodicity in R_B/R_{SUN}, 11.9 years, and the average periodicity of the GSS between 1700 and 2015, 11.03 years. When the correlation coefficient between GSS and R_B/R_{SUN} for the eight planet system is found by a similar analysis for the same time interval the correlation coefficient is 0.034. A heliographic inertial longitude of $L_9 = 60°$ locates Planet 9, at the present time, in the vicinity of the constellation Leo, near right ascension ~11 hours, declination ~+15°.

4. Comparing the Centennial Scale Variation of SSN and R_B/R_{SUN}

Grand solar minima tend to occur in clusters associated with minima in the ~2400 year Hallstaat cycle [22]. The most recent minimum of the Hallstatt cycle and most recent cluster of grand solar minima occurred during the last millennium [22]. Figure 7 plots the centennial time scale average value of R_B/R_{SUN} for the nine planet system for different values of Planet 9 longitude in this time interval. Figure 7 shows that the timing of minima in the centennial scale variation of R_B/R_{SUN} is sensitive to variation of Planet 9 longitude and that when the Planet 9 longitude is close to 60° the occurrence times of the minima in R_B/R_{SUN} are consistent with the times of occurrence of the most recent grand solar minima in SSN, indicated by the vertical reference lines. The times of the recent grand solar minima are taken from the estimates of the central times of grand solar minima [44] [45]: Maunder, 1680, Sporer, 1473, Wolf, 1316, and Dalton 1815. The time for the Modern grand minimum, 2030, is an estimate [46]-[51].

It is interesting to compare the result in Figure 7 with the analysis of Feynman and Ruzmaikin [47] who analysed the SSN record from 1700 to 2010 and
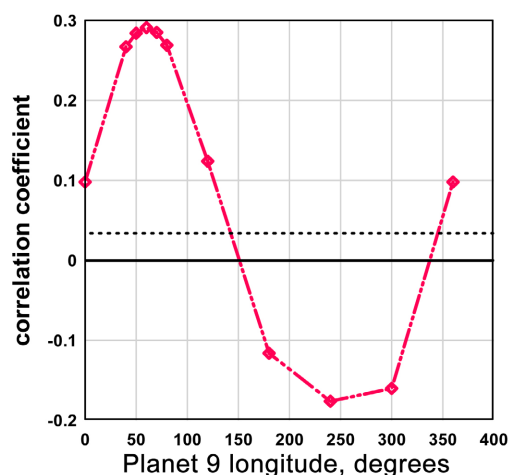

Figure 6. The correlation coefficient between the GSS variation and the R_B/R_{SUN} variation between 1700 and 2015 as the heliographic inertial longitude of Planet 9 varies. The dotted reference line indicates the level of correlation, 0.034, between the GSS variation and the R_B/R_{SUN} variation for the eight planet system.
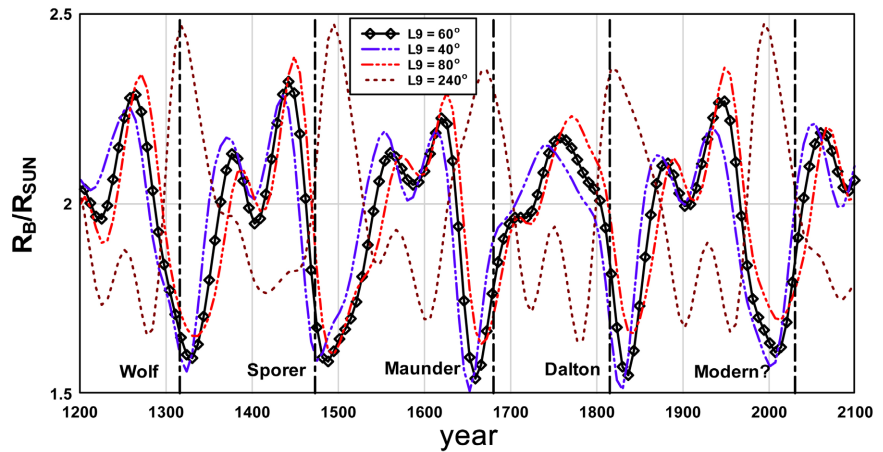
Figure 7. Shows the centennial scale variation of R_B/R_{SUN} between year 1200 and year 2100 for different values of the heliographic longitude, HGIL9, of Planet 9. The data, obtained at 6.5 year intervals, has been averaged over 33 years to emphasise the ~172 and ~86 year components, see the spectrum of **Figure 2**. The vertical reference lines correspond to dates at the centre of grand solar minima taken from [45]. The date for the Modern minimum is an estimate.

associated grand solar minima as being due primarily to the ~88 year Gleissberg cycle. **Figure 7** clearly indicates that the centennial variation of R_B/R_{SUN} is due to the interference of the ~172 year and ~86 year components. As a result R_B/R_{SUN} sharply decreases when the negative phases of the two components interfere constructively. The decreases are separated by broad maxima, occasionally containing a weak minimum, where the positive phase of the ~172 year cycle interferes with negative phase of the ~86 year cycle. The variation in R_B/R_{SUN} in **Figure 7** is also consistent with the recent reconstruction of SSN over the last millennium [45], particularly in respect to the occurrence of grand minima and the occurrence of weak minima between the grand minima. For example, from **Figure 7** weak minima in SSN would be expected near years 1400 and 1900. This expectation is consistent with recent observations of SSN [45].

As noted earlier when Planet 9 is included in the solar system the ~172 year period component is increased by a factor ~10 and the ~86 year component, previously not present, appears strongly in SIM, c.f. **Figure 2**. It is therefore interesting to follow, in terms of SIM about the barycentre, why the introduction of Planet 9 leads to such large centennial scale variations in R_B/R_{SUN}. **Figure 8** illustrates how the orbital pattern of the Sun about the barycentre, (0,0), varies between an interval centred on a centennial scale grand minimum in R_B/R_{SUN}, here 1627 to 1703, and an interval between centennial scale grand minima in R_B/R_{SUN}, here 1880 to 1964.

5. Comparison of the Millennial Scale Variation of Reconstructed SSN and R_B/R_{SUN}

5.1. The Millennial Scale Variation of R_B/R_{SUN}

The variability of solar activity over timescales longer than several centuries can
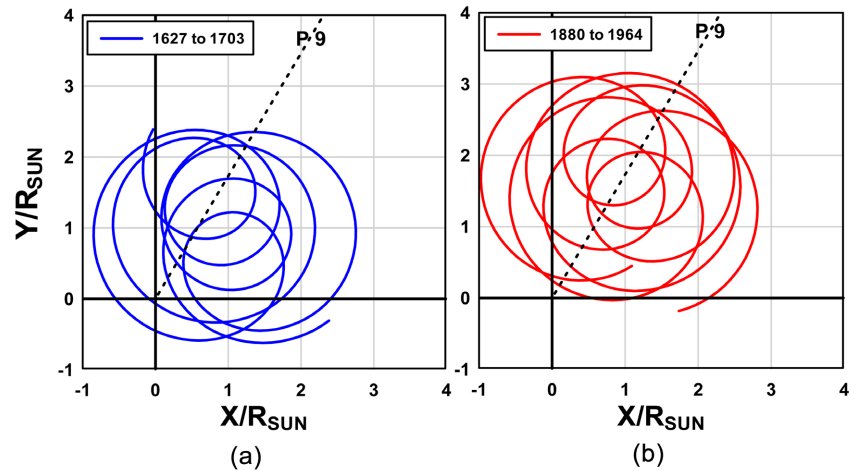
Figure 8. In both (a) and (b) the origin is at the barycentre and the paths indicate the motion of the Sun. (a). During a grand solar minimum, here the Maunder Minimum, 1627 to 1703, the known outer planets, Uranus, and Neptune, both lie at longitudes in the lower left quadrant, *i.e.* are in inferior conjunction, while Planet 9 lies along the longitude, 60˚, indicated by the dotted line in the upper right quadrant. As a consequence the orbital pattern of the Sun about the barycentre, indicated in (a), is shifted toward the barycentre and the centennial scale average Sun to barycentre distance is decreased as compared with times when, as in the time interval 1880 to 1964, (b), Uranus and Neptune are near superior conjunction, one in the lower left quadrant and the other in the upper right quadrant, and Planet 9 displaces the orbital pattern away from the barycentre. Note that, in both diagrams, the orbital pattern shown is due to the effect of the planets Jupiter, Saturn, Uranus, and Neptune and this pattern, in the absence of Planet 9 would be centred on the origin. The effect of Planet 9 is simply to displace the pattern away from the origin or the barycentre of the solar system.

only be studied by proxy records of solar activity derived from measurements of the concentration of the cosmogenic isotopes, radiocarbon ^{14}C in tree trunks and [10]Be in polar ice, that accumulated due to the effect of cosmic rays [22] [52] [53] [54] [55]. Due to the inverse relationship between cosmic rays and solar activity it was possible to reconstruct the variation of SSN over the approximately 9,000 year Holocene interval, −7000 BC to 2000 AD [22] [56]. Analysis of the record shows a variation, nominally the Hallstatt cycle, of periodicity about 2400 years. The Hallstatt cycle and a longer period cycle were also observed in the ^{14}C record [13]. Usoskin *et al.* [22], concluded that the ~2400 year Hallstatt cycle is most likely a property of long term solar activity. They show, by superposed epoch analysis that grand minima in SSN tend to cluster at minima of the ~2400 year cycle. The ~2400, ~1000, ~85, ~60 and ~30 year period components are important components in solar activity, cosmic ray flux and cosmogenic series and have been extensively reported [13] [20] [22] [55] [57] [58]. In this section we show that the spectral content of R_B/R_{SUN}, calculated when Planet 9 is included, exhibits the Hallstatt ~2400 year cycle, the Gleissberg ~88 year cycle, the ~60 year cycle, and the ~30 year cycle, **Figure 9(a)**. Conversely, in the spectrum of R_B/R_{SUN}, calculated without Planet 9, these long term components of reconstructed solar activity are insignificant, **Figure 9(b)**.
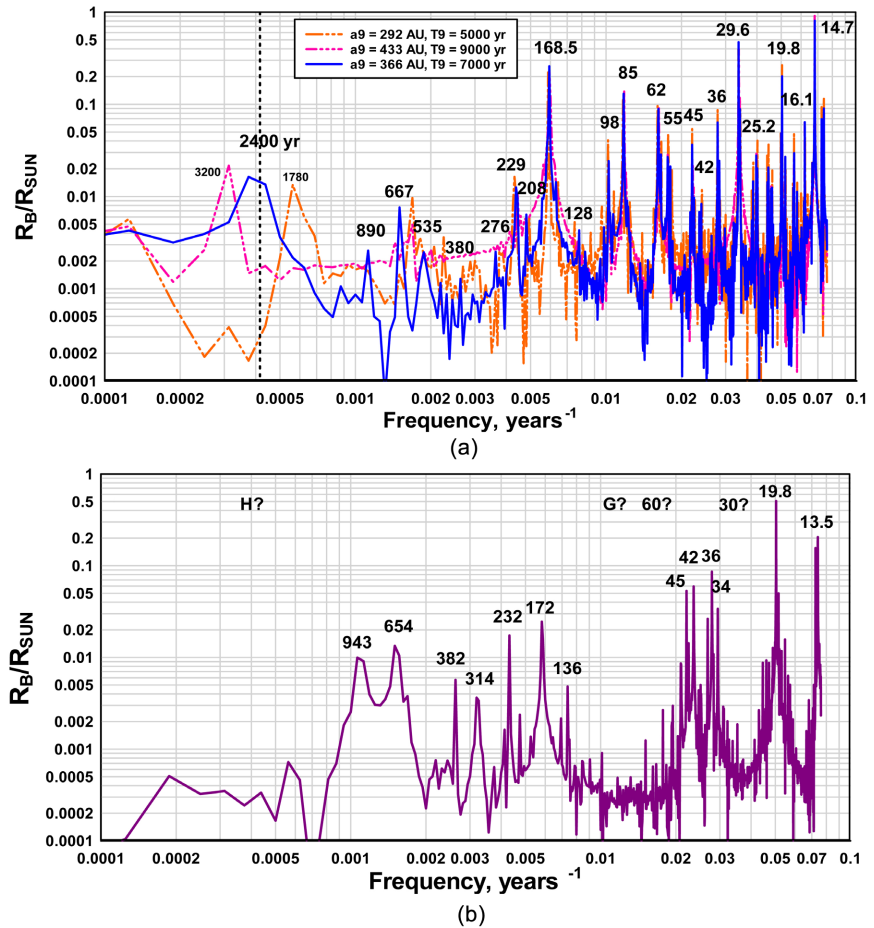
Figure 9. (a) Shows the tuning of the low frequency, long period, cycle in R_B/R_{SUN} to the nominal Hallstatt period, ~2400 years, by varying the orbital period of Planet 9 to T_9 = 7000 years. (b) The components of the spectral content of R_B/R_{SUN} for the eight planet system show no evidence of either the Hallstatt, ~2400 year, Gleissberg, ~88 year, ~60 year, or ~30 year period components.

Figure 9(a) and **Figure 9(b)** compare the spectral content of R_B/R_{SUN} for the eight planet and nine planet systems when assessed between year −8000 and year +8000. Three overlapping nine planet spectra are shown in **Figure 9(a)**. Each spectrum is for a different value of semi-major axis and the corresponding Planet 9 orbital period. Clearly, the low frequency components of R_B/R_{SUN} are sensitive to changes in Planet 9 semi-major axis and period. Therefore the variation of Planet 9 period provides a means to fit the lowest frequency component of R_B/R_{SUN} to the previously observed ~2400 year period of the Hallstaat cycle in reconstructed SSN by varying the orbital radius or orbital period of Planet 9. **Figure 9(a)** indicates that a close fit is obtained with a_9 ~ 366 AU, or equivalently, since T and a are related, T_9 ~ 7000 years. The value a_9 ~ 366 AU is close to the best estimate value, a_9 = 380 AU obtained by [1].

Figure 10 compares the eight planet and the nine planet time variations of R_B/R_{SUN} from year −8000, (8000 BC) to year +8000, (8000 AD). The points are calculated at 2400 day intervals so that the label S5 indicates a running average
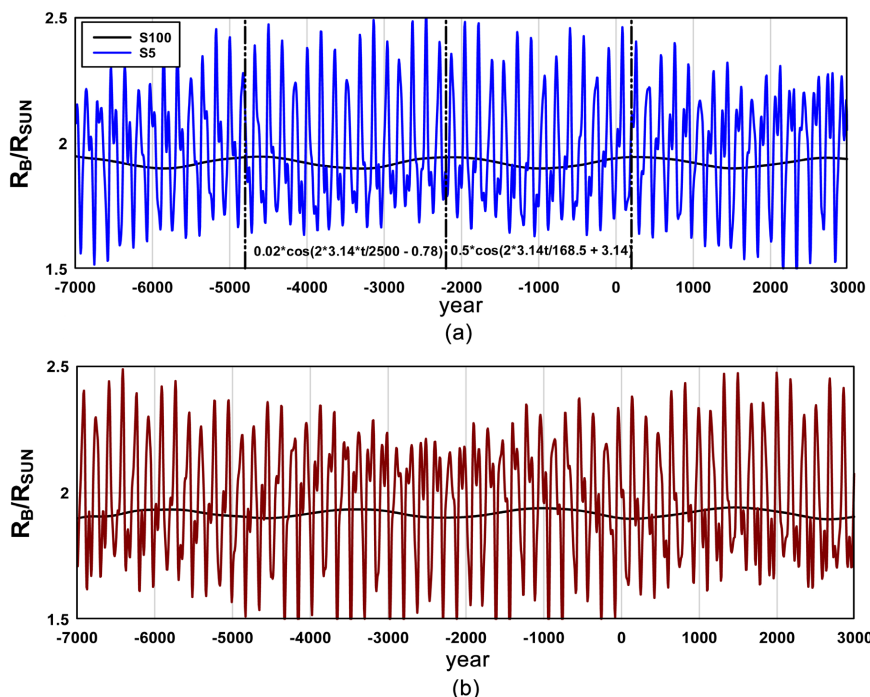
Figure 10. (a) The millennial scale variation of R_B/R_{SUN} for $a_9 = 366$ AU and $L_9 = 60°$. The label S5 corresponds to a running average over 33 years and the label S100 corresponds to a running average over 660 years. The vertical reference lines in (a) correspond to times of maxima in the second singular spectral analysis component, nominally the Hallstaat cycle component, in reconstructed sunspot number [22]. (b) The same variations as in A with $L = 240°$. Notice that the phase angle of both the short term ~170 year cycle and the long term ~2400 year cycle shift by 180° when the longitude of Planet 9 changes by 180°. The best fit to the higher frequency component in (A), nominally the Jose component, is $R_B/R_{SUN} = 0.5\cos(2\pi t/168.5 + \pi)$ and the best fit to the low frequency component, nominally the Hallstatt component is $R_B/R_{SUN} = 0.02\cos(2\pi t/2500 - 0.78)$. This Hallstaat component in R_B/R_{SUN} has its most recent minimum value at year 1560 in (A).

over 5 points or a 12,000 day, 33 year interval and the label S100 indicates a running average over a 660 year interval. There is a very strong centennial time range cycle of ~170 year period and a weaker millennial time range cycle of ~2400 year period. Comparing **Figure 10(a)** where $L = 60°$ and **Figure 10(b)** where $L = 240°$ indicates that the ~2400 year cycle is sensitive to change in Planet 9 longitude, *i.e.* the phase of the ~2400 year cycle shifts by 180° when the longitude of Planet 9 shifts by 180°.

The type of variation in **Figure 10** arises when the major components, in this case the ~176 year and ~88 year period components are not exactly harmonically related. If the two components are harmonically related as suggested by the ratio 176/88 = 2.0 then a stationary pattern would result rather than the slowly varying pattern in **Figure 10**. Assuming the longer period component derives from the Uranus-Neptune conjunction period of 172 years we expect the synoptic period of the conjunction Uranus/Neptune/Planet 9 (period ~7000 years) to be 176.5 years and for the synoptic period of the harmonic of 172 years (86 years) to occur at 87.0 years. Thus Planet 9 results in a period ratio of 176.5/87.0 = 2.03

for the two components rather than exactly 2.00 and the difference in period from exact harmonic ratio is sufficient to give the slowly varying pattern in **Figure 10**.

5.2. The Millennial Scale Variation in Spectral Content of SSN

The spectral content of the reconstructed SSN, −6755 to 1885, shown in **Figure 11** was obtained after removing a running average over 2400 years from the reconstructed SSN [56]. The spectrum is similar to that obtained with ^{14}C data [59].

It is clear by comparing the spectrum of SIM, **Figure 9(a)** and the spectrum of SSN, **Figure 11** that the hypothetical transformation of SIM into sunspot emergence, if it exists, acts as a low pass filter, *i.e.* the transform of cycles of SIM into cycles of sunspot emergence is much stronger at low frequencies than at high frequencies. The periods of reconstructed SSN in **Figure 11** along with the apparently corresponding periods of R_B/R_{SUN} in brackets are: 2160 (2400), 1440 (?), 960 (890), 720 (667), 617 (?), 508 (535), 346 (380), 206 (208), ??? (168), 149 (?), 133 (?), 104 (98), 87 (85), 68 (62), 53 (55), 43 (45), 38 (36), 33 (?), 29 (29.6). Where there is no apparent correspondence a question mark is placed. Note that the three question marks indicate the absence of the ~168 year Jose component from the SSN record. Clearly there is a reasonably close correspondence between the low frequency periodicity of SIM and reconstructed SSN apart from the Jose component that is marked with the dotted reference lines in **Figure 11**. This issue, which challenges the hypothesis of a connection between SIM and solar activity, is discussed in detail below.
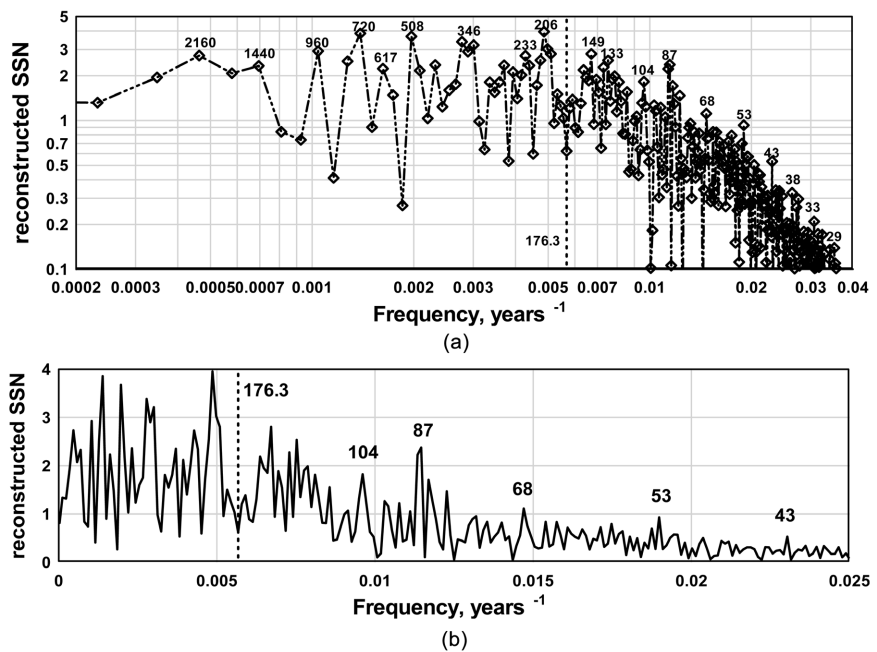

Figure 11. The spectral content of the reconstructed SSN record [56]. The periods, in years, of prominent peaks are labelled. The location of the ~176 year Jose periodicity, which is absent from the spectrum, is marked by the vertical dotted reference line.

6. Phase Modulation of the ~170 Year Jose Periodicity by Lower Frequency Components

6.1. Elements of Phase Modulation and Demodulation

The modulation of a high frequency signal by a lower frequency signal is the basis of communication engineering where the higher frequency signal is called the carrier and the lower frequency signal is called the modulation. The basic types of modulation used in communications are amplitude modulation and phase/frequency modulation. The same concept has been applied to investigating the spectral content of solar activity and climate variables, e.g. amplitude modulation [60] and phase/frequency modulation [61] [62]. In amplitude modulation a fraction of the power at the carrier frequency is shifted into sidebands on either side of the carrier frequency while in phase/frequency modulation most of the power is shifted from the carrier frequency into sidebands of the carrier frequency. The latter occurs, for example, in the modulation of the annual cycle of the interplanetary magnetic field by the ~22 year Hale cycle, where all the power in the annual cycle is shifted into sidebands [61]. So a characteristic of the spectra resulting from phase/frequency modulation is a distinct minimum at the carrier frequency and strong sidebands spaced equally at each side of the carrier frequency. There is a deep minimum at ~170 years in spectrum of reconstructed sunspot number, Figure 11. A possible explanation for the absence of the Jose periodicity at ~170 years from the spectrum is that the Jose periodicity is split into sidebands by phase modulation by lower frequency components. We investigate this possibility in the following.

Modulation of a carrier signal of angular frequency, ω_C, by a lower angular frequency, ω_M, modulating signal can be represented by

$$y(t) = \left[A + \cos(\omega_M t)\right]\cos(\omega_C t)$$

$$y(t) = A\cos(\omega_C t) + 0.5\left[\cos\left((\omega_C + \omega_M)t\right) + \cos\left((\omega_C - \omega_M)t\right)\right]$$

$$y(t) = A\cos(\omega_C t) + 0.5\left[\cos(\omega_H t) + \cos(\omega_L t)\right] \tag{5}$$

where ω_H and ω_L are the angular frequencies of the high and low frequency sidebands respectively. When $A > 1$ we have amplitude modulation, $A < 1$ partial amplitude and phase modulation, and $A = 0$, pure phase modulation where on every second half cycle of the modulating signal the phase of the carrier signal is reversed. If f_H and f_L can be found the modulating frequency is,

$$f_M = (f_H - f_L)/2 \tag{6}$$

and the carrier frequency is,

$$f_C = (f_H + f_L)/2 \tag{7}$$

When $A = 0$ we have pure phase modulation. As an example, if there are two components in the modulating signal, at periods 1500 years and 600 years, and the carrier period is 168 years, the Jose periodicity, the modulated wave form and the spectrum are as shown in Figure 12(a) and Figure 12(b).
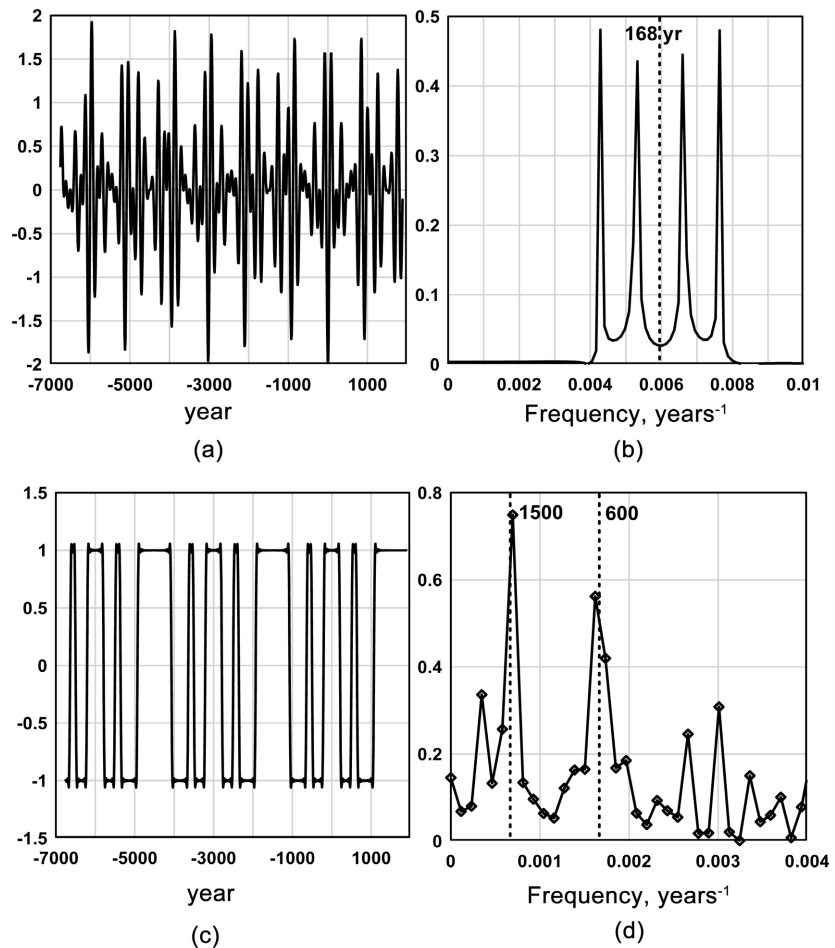
Figure 12. The figures illustrate the method of demodulating a phase modulated signal in order to reveal the low frequency modulating signal. (a) is the phase modulated signal. (b) is the spectrum of (a). The modulating periods could be obtained by applying equation 6 to the components in (b) to find the modulating periods. However, it is possible to de-modulate the signal (a) by correlating signal (a) with the carrier signal, in this simulation, $\cos(2\pi t/168)$. The result is the low frequency waveform (c), corresponding to in-phase and out-of-phase intervals of signal (a) with the carrier signal. Obtaining the spectrum of (c) by FFT recovers the periods of the low frequency modulating components, (d).

In this case, the carrier frequency is easy to determine as the midpoint frequency between the sidebands in the spectrum. If the carrier period and the carrier phase are known, the low frequency modulating waveform can be recovered by demodulating the modulated signal, the variation in (A) in the **Figure 12**. Demodulation is obtained by correlating the modulated signal with the carrier signal, in the above simulation the carrier signal was $\cos(2\pi t/168 + 0)$. The result of the demodulation is shown in **Figure 12(c)** which is indicative of the modu-lated signal alternating between in-phase and out-of-phase with the Jose cycle. The spectrum of the demodulated signal is shown in **Figure 12(d)**. Note that periods of the original modulating cycles, 1500 year and 600 year, are, by this process, recovered from the modulated waveform. Clearly the demodulation method is not exact and weak spurious components are generated as evident in

Figure 12(d). It is also possible, by using slight variations in period and phase of the Jose cycle, and the above simulation methods, to show that the demodulation method is very sensitive to the period and phase of the Jose cycle.

6.2. Phase Modulation and Demodulation Applied to the Reconstructed Sunspot Number

It is clear from the above that it is possible to move back and forth between a modulated signal and the modulating signal. We now apply this method to the reconstructed SSN record [56] with the objective of demonstrating the possibility that the Jose cycle is the "hidden" mediator between the low frequency and mid frequency components of the SSN record. **Figure 13** outlines the transformation by which the low frequency components of the SSN variation modulate
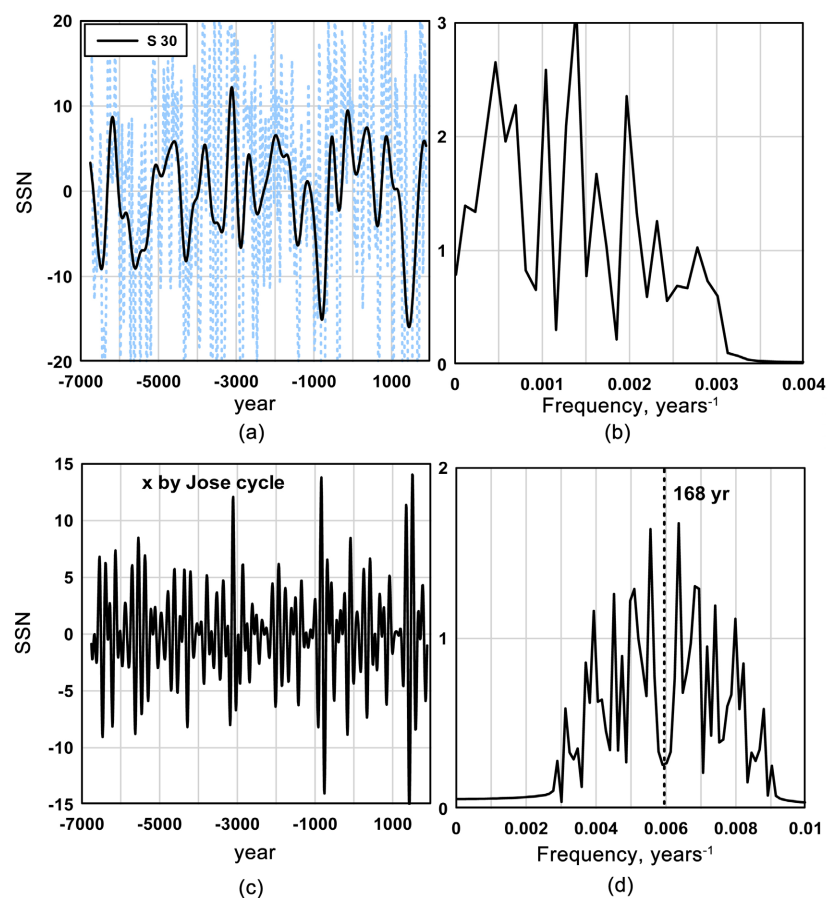

Figure 13. The figures illustrate the modulation of the Jose cycle by the low frequency components in the reconstructed SSN record. The blue broken curve in (a) is the time variation of the reconstructed SSN record −6755 to 1885 [56]. The full line is the low frequency component obtained by a 300 year running average. The spectrum of the low frequency SSN variation is shown in (b). If the low frequency time variation in (a) modulates a Jose cycle, $\cos(2\pi t/168 + \pi)$, the resultant mid frequency SSN variation is shown in (c). The spectrum of this mid frequency variation, shown in (d), is characterised by a deep minimum centred on the Jose periodicity, comparable with the spectrum of **Figure 11(b)**. The sidebands correspond to phase modulation of the Jose cycle by the low frequency components of the time variation in (a).

the Jose cycle and result in the mid frequency components of the SSN. The very low frequency component of SSN record, period longer than ~2400 years, that Usoskin *et al.* [22] regarded as likely being of terrestrial origin, was removed by subtracting a 2400 year running average. This resulted in the very complex blue broken curve shown in Figure 13(a). A running average over 30 points, or 300 years, was then used to obtain the low frequency waveform, the full line in Figure 13(a). The spectrum of this low frequency SSN waveform, shown in Figure 13(b), has seven significant low frequency components. Figure 13(c) is the result of modulating the Jose cycle, $\cos(2\pi t/168 + \pi)$, obtained from Figure 10(a), with the low frequency waveform of Figure 13(a). The resulting spectrum, corresponding to variation in the mid frequency range of the SSN record is shown in Figure 13(d), the most noticeable feature being the distinct minimum in spectral amplitude centred on the Jose period, 168 years. This spectrum, Figure 13(d), is directly comparable, in the same frequency range with Figure 11(b), which shows the entire SSN spectrum. The sidebands in Figure 13(d) are evidently the result of phase modulation of the Jose cycle by the low frequency components present in the variation in Figure 13(a). For example the most central pair of sidebands in 13 D is due to modulation by the 0.0005 year^{-1}, ~2000 year, component in Figure 13(a) and the second set of sidebands from the centre is due to phase modulation by the ~1000 year component in Figure 13(a).

We now demonstrate the demodulation of the SSN record in the mid frequency range via correlation with the Jose cycle to obtain the low frequency components of the reconstructed SSN record [56]. The mid frequency range variation of the SSN record is obtained by using a digital band pass filter to isolate the time variation of SSN in the frequency range from 0.003 years^{-1} to 0.009 years^{-1}, Figure 14(a). The spectrum of this variation, shown in Figure 14(b), has all the low frequency components of the SSN variation removed by the filter. We now correlate the mid frequency range variation, Figure 14(a), with the Jose cycle, $\cos(2\pi t/168 + \pi)$, as determined in Figure 10(a). The variation of the resulting correlation coefficient, after smoothing with a 100 year running average, is shown in Figure 14(c). The spectrum of this variation, shown in Figure 14(d), contains low frequency components similar in period to the low frequency components of the SSN record in Figure 13(b).

The time variation in Figure 14(c) and the spectrum in Figure 14(d) are reasonably consistent with the low frequency time variation of Figure 13(a) and the low frequency spectrum of Figure 13(b), indicating that the demodulation of the mid frequency range variation in the SSN record with the Jose cycle is recovering, to a reasonable approximation, the low frequency time variation of the reconstructed SSN record. The effectiveness of the type of transformations illustrated in Figure 13 and Figure 14 support the concept that phase modulation of the Jose cycle in SIM by the low frequency components in SIM results in the mid frequency range variation of the reconstructed SSN. It also explains the occurrence of the deep minimum in the spectrum of the SSN record at ~170 years period that is evident in the spectrum of reconstructed SSN, Figure 11(a) and
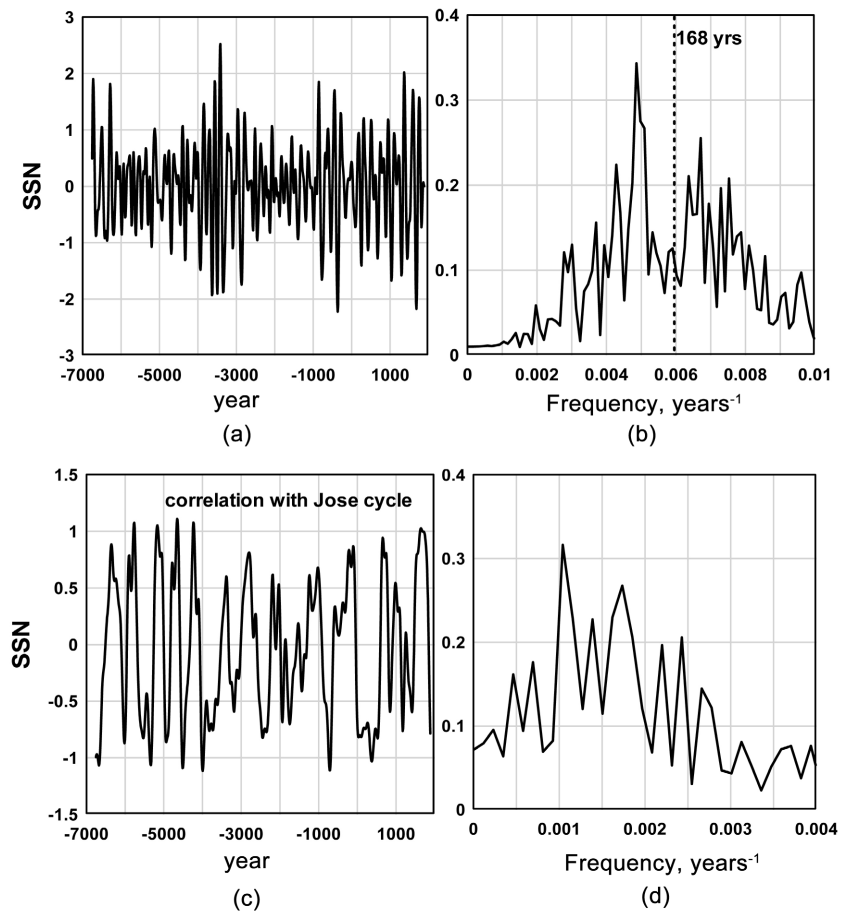
Figure 14. The figures illustrate the demodulation of the mid-frequency SSN record to obtain the low frequency components of the reconstructed SSN record [56]. The variation in (a) is the mid-frequency variation of the SSN record obtained by digital band pass filtering. The spectrum in (b) is the result of a FFT of time variation in (a) and shows the deep minimum at about 0.006 years^{-1} characteristic of phase modulation of a component at that frequency. (c) shows the correlation of the time variation in (a) with the Jose cycle $\cos(2\pi t/168 + \pi)$ after smoothing with a 100 year running average. (d) shows the FFT of the time variation in (c) and corresponds to the spectrum of the low frequency components of the SSN record and is directly comparable with the spectrum in **Figure 13(b)**.

Figure 11(b), and in previous observations of the spectral content of cosmogenic isotope series [55] [60] [63]. Note that in a later section, Section 6.4, we find that the Jose periodicity in SIM varies slightly with Planet 9 orbital radius and, if the Planet 9 orbit is eccentric, an exactly constant Jose periodicity may not apply to SIM.

The hypothetical connection between SIM and SSN is that SIM, by some mechanism, as discussed below, induces changes in the magnetically active region of the Sun that vary the rate of emergence of sunspots. The connection between SIM and the reconstructed SSN involves several further connections. Connections between sunspots and solar wind, solar wind and cosmic rays, cosmic rays and the production of ^{14}C or ^{10}Be isotopes, the accumulation of the isotopes in tree rings or ice layers, the interpretation of tree rings and ice layers

into a time sequences, and the conversion of the resulting cosmogenic time series into a proxy record of sunspot emergence [56]. In view of the noise, nonlinearities and uncertainties involved in such a complex process it is unlikely that the analysis, outlined above, based on phase modulation of the Jose cycle, Figure 13 and Figure 14, would yield a very close resemblance between the observed and estimated low and mid frequency components of the reconstructed SSN. Nevertheless the comparison is, on close examination, reasonably convincing and we conclude, tentatively, that in the transformation from SIM to solar SSN, the Jose cycle in SIM is phase modulated in the process and that this phase modulation could be the reason for the absence of Jose periodicity in the spectra of SSN.

6.3. Spectral Analysis from the Occurrence of Grand Solar Minima

Grand solar minima have been a preoccupation of solar and climate researchers since the reporting of the Maunder solar minimum by Eddy [20]. The study of grand solar minima is important in the context of understanding the origin of long term variations in the solar dynamo [15] [18] [22] [64] [65] and in relation to the possible climate impacts of grand solar minima, e.g. [55] [66] [67] [68] [69]. The cosmogenic record has enabled the study of the occurrence of grand solar minima over the last ten millennia with [44] reporting the centre times of grand minima in the reconstructed SSN and [53] reporting the centre times of grand minima in the solar modulation potential. The conclusions of the latter two studies is that, "*the occurrence of grand minima and maxima is not a result of long-term cyclic variability but is defined by stochastic/chaotic processes*" and "*other than a weak quasi-periodicity of 2000-2400 years… No other periodicities are observed in the occurrence rate of grand minima*" [44]. The conclusions are counter to the findings in this section that grand solar minima result from the phase modulation of the ~170 year Jose cycle by lower frequency cycles such as the ~1000 year Eddy and ~2400 year Hallstatt cycles. However, Inceoglu *et al.* [64] have changed their view about grand solar minima to, "*it would also imply that these quiescent periods of activity are not the result of a random process but instead their origin is linked to the driving mechanism of magnetic field generation*".

With a view to assessing if long term cyclic variability is present or not in the occurrence of grand minima we here study the central dates of grand solar minima observed by [44] [53]. The objective is to assess if the ~170 year Jose cycle and the harmonic and sub harmonics of the Jose cycle are evident in the occurrence dates. The method is to specify, in the relevant time interval, a value unity for the centre years of grand solar minima and a value of zero for all other years. To enable the use of FFT analysis the central dates of grand solar minima are assigned to the nearest fifth year in the sequence of years between −9200 and 1810 and given the value unity. The sequence, after smoothing with a ten year running average, and representing the occurrence of grand minima as specified by [44] or [53], is shown in Figure 15(a) for the [44] data and Figure 16(a) for
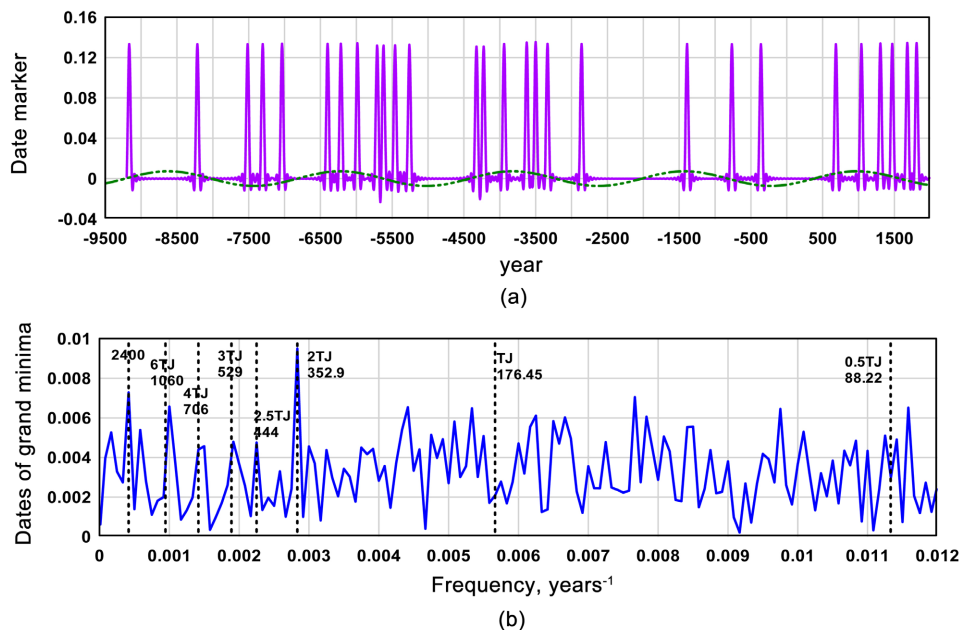
Figure 15. (a) The time sequence of the central dates of solar grand minima obtained by [44]. (b) The spectral content of the time sequence in (a). The strongest peak, at 352.9 years, is assigned the value 2TJ, where TJ is the Jose period in SSN. TJ is then calculated to be 176.45 years and this period is indicated by the TJ reference line. The harmonic and sub harmonics of the Jose components are then indicated by reference lines. The peak that occurs at period 2400 years is also indicated.
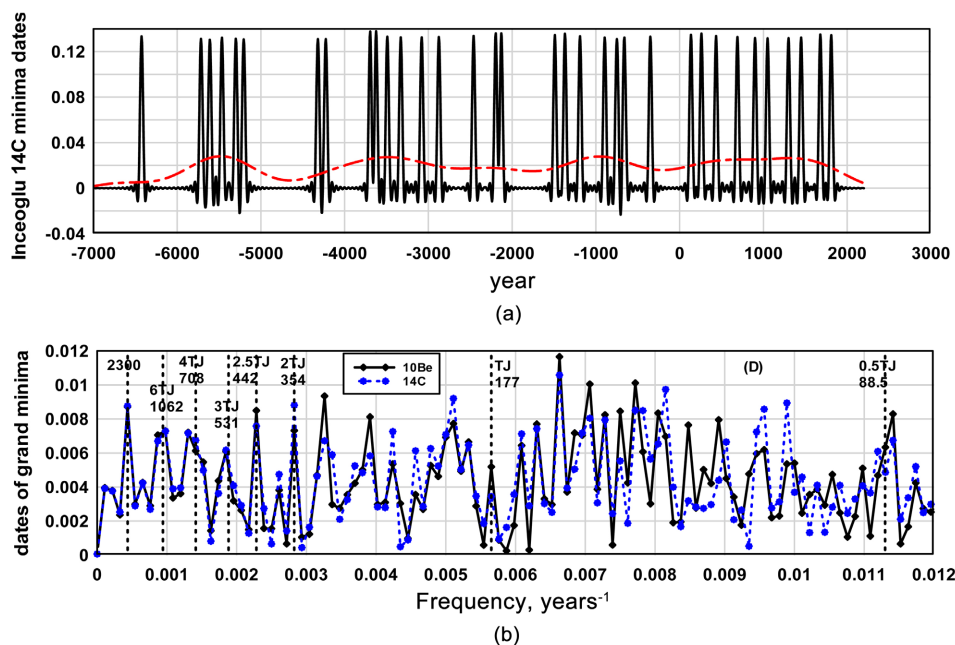
Figure 16. Upper graph. The time sequence of the central dates of solar grand minima in the ^{14}C record of solar modulation potential obtained by [53]. Lower graph. The spectral content of the time sequences in ^{14}C and ^{10}Be solar modulation potential. The strong peak, at 354 years, is assigned the value 2TJ, where TJ is the Jose period in SSN. TJ is then calculated to be 177 years and this period is indicated by the TJ reference line. The harmonic and sub harmonics of the Jose components are then indicated by reference lines. A peak at 2300 years is also indicated.

the [53] data. A fast Fourier transform of the sequence is then made to identify periodicities in the sequences, **Figure 15(b)** and **Figure 16(b)**. This method is similar to that applied to uncover the spectral content of ground level enhancement events [70]. The strongest peak in the spectrum of the data recorded in [44] is at 352.9 years. We associate this period with 2TJ where TJ is the Jose periodicity, 176.45 years. As expected from the discussion about phase modulation, a prominent peak at period TJ is not evident in the spectrum and the period TJ is associated with a deep broad minimum in the spectrum. Four sub-harmonics, at periods 2.5TJ, 3TJ, 4TJ, and 6TJ coincide with prominent peaks and are indicated with reference lines. The first harmonic of the Jose periodicity at 0.5TJ = 88.22 years is also indicated. The long term periodicity at ~2400 years that represents the clustering of solar grand minima occurrences is also marked. Note that the ~2400 year cycle of clusters of grand solar minima in **Figure 15(a)** corresponds to the clusters occurring within the negative phase of the ~2400 year Hallstatt cycle in SIM in **Figure 10(a)**.

The analysis is repeated for the reconstructions of solar modulation potential from the ^{10}Be and ^{14}C cosmogenic series [53]. This sequence of grand solar minima occurrences is shown in **Figure 16(a)** and the resulting spectral content of the occurrences is shown in **Figure 16(b)**. The periodicities marked by reference lines are essentially the same as in the spectrum of **Figure 15(b)** derived from the [44] data. Thus three different estimates of the occurrence of grand minima give essentially the same periodicity of occurrence and that periodicity is dominated by a Jose periodicity of ~177 years and sub harmonics of this periodicity.

The ~177 year Jose periodicity in the occurrence of solar grand minima, while clearly associated with the low frequency components in the spectrum is "hidden" in the sense that the amplitude of the component is relatively weak compared with the amplitude of the sidebands and with the amplitude of lower frequency components. This is a result, as outlined in Section 6.2, of phase modulation of the Jose component by lower frequency components. However, the phase modulated component is not completely "hidden" if the number of phase reversed cycles or events differs significantly from the number of regular cycles or events. In the context of grand solar minima occurrences, if all grand minima occurred at $n \times 176$ year intervals in the time sequence then there would be a strong peak at 176 years in the spectrum of occurrences. If, however, about half of the grand minima occurred at $(n + \frac{1}{2}) \times 176$ year intervals in the time sequence the 176 year periodicity in the spectrum would be "hidden". In the spectrum of **Figure 16(b)** a peak at ~177 years is evident but relatively weak indicative of an imbalance between in phase and out-of-phase occurrences of grand solar minima. There are several strong peaks in the spectrum that correspond to phase modulation of the Jose cycle that have not been marked by reference lines. For example, using Equations (6) and (7), the peaks at 303 years, (0.0033 years^{-1}), and 256 years, (0.0039 years^{-1}), in **Figure 16(b)** are sideband peaks due to phase modulation of the Jose cycle by the 442 year period and 531 year period

low frequency components respectively. Similarly the strong, broad peaks at ~0.005 year^{-1} (200 years) and ~0.007 years^{-1} (143 years) are sideband peaks due to phase modulation of the ~177 year Jose cycle by the ~1000 year Eddy cycle.

Beer *et al.* [27] suggested that solar grand minima "recur with the characteristic de Vries period of approximately 208 years" and supported this idea by band pass filtering the cosmogenic ^{14}C record in the period range between 180 and 230 years, further stating that the maxima in the filtered cosmogenic record "*actually correspond to grand minima in solar activity*". The evidence of Figure 16(b) suggests that the recurrence time of solar grand minima obtained from the ^{14}C record is close to 177 years. If the recurrence time was 208 years a peak at 0.0048 years^{-1} would be evident in the spectrums in Figure 15(b) and Figure 16(b).

The above analysis is presented as a possible reason why the Jose periodicity, a dominant periodicity in the spectrum of SIM, is absent from the spectrum of reconstructed SSN whereas other periodicities in SIM, e.g. the ~2400 year Hallstatt, ~1000 year Eddy, and the ~88 year Gleissberg periodicities, are clearly present in the spectrum of reconstructed SSN, c.f. Figure 11(a) and Figure 11(b).

Another conundrum in this attempt to relate SIM to SSN is the discrepancy between the ~177 year Jose periodicity obtained by spectral analysis of the solar activity record, Figure 11(a) and Figure 16(b), and the ~170 year Jose periodicity obtained from SIM, Figure 9(a) and Figure 10(a). Sharp [71] and McCracken *et al.* [32], using very long records of SIM, estimated the Jose period to be ~171 years as opposed to the estimate by Jose (1965), over the short interval 1653 to 2060, of a Jose period of ~about 178 years. The estimate obtained in this paper using the approximation of circular planet orbits is a period ~169 years for SIM including Planet 9 and a period ~172 years for SIM for the eight planet system, the latter value consistent with the estimate by Sharp [71] and McCracken *et al.* [32]. The discrepancy between ~177 years for SSN and ~170 years for SIM is large enough to be a significant challenge to the planetary hypothesis.

6.4. Why Are the Jose Periodicities in SSN and SIM Different?

The previous section found the "hidden" Jose periodicity in SSN is ~176.5 years, Figure 15 and Figure 16, whereas the calculated Jose periodicity in SIM was ~168.5 years, Figure 9(a). This discrepancy may be resolved by noting that the Jose periodicity in SIM varies with the semi-major axis, a_9, of Planet 9, Figure 17.

In fact all of the SIM periodicities that depend on the semi-major axis of Planet 9 vary. The Gleissberg ~88 year periodicity in SIM also decreases with a_9, Figure 17. However, in contrast, the Hallstaat periodicity in SIM increases strongly with a_9, Figure 9(a). Thus, a possible resolution of the difference between the SSN and SIM estimates of Jose periodicity is that the orbital radius of Planet 9 used in the calculation of SIM in this paper, 380 AU, the best estimate from [1], is actually shorter, about 250 AU.
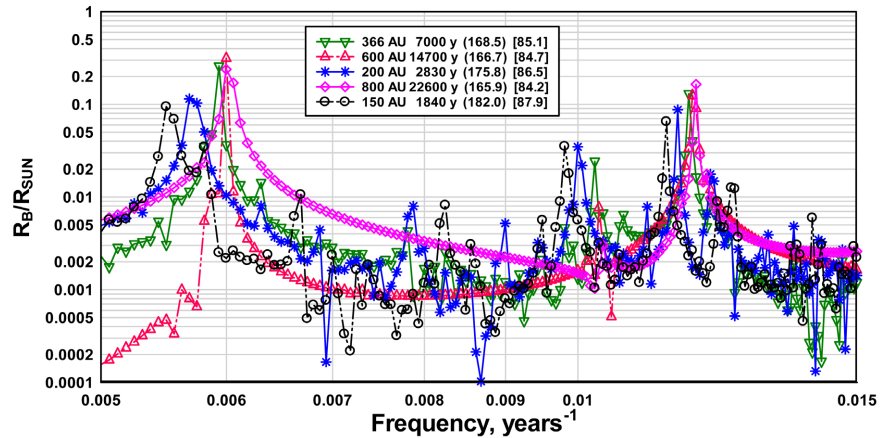
Figure 17. The spectral content of R_B/R_{SUN} as the semi-major axis of Planet 9 is varied between 150 AU and 800 AU. Note that all the periodicities move to lower frequencies as the Planet 9 semi-major axis decreases. The semi-major axis and orbital period of Planet 9 are given in the legend as is the period, in years, of the Jose cycle in SIM, indicated by the number in (…), and the period of the Gleissberg cycle in SIM, indicated by the number in […].

Another possibility is that the Planet 9 orbit is eccentric of the order e ~ 0.3, and the occurrence of grand solar minima cluster around the times of perihelion when the orbital radius approaches a lower value of 250 AU. In this case most of the solar grand minima in SSN would be expected to occur, in clusters, at a time spacing of about 176 years, as observed, corresponding to the Jose periodicity in SIM when a_9 ~ 250 AU, also ~period 176 years.

7. Mechanism for the Conversion of SIM into SSN

There is a conundrum that, while there is reasonably close correspondence between most of the significant periodicities in SIM and in SSN, the principal component in SIM, the ~170 year Jose periodicity, is not evident in spectra of reconstructed SSN or in cosmogenic records [55]. The inclusion of Planet 9 in the solar system results in broad decreases in R_B/R_{SUN} coherent with the occurrence of grand solar minima, c.f. **Figure 1** and **Figure 7**. The significant long term, ~170 year period, variation in R_B/R_{SUN} implies that the Sun is subject to intervals of extreme positive and negative acceleration relative to the barycentre with the intervals separated by ~170 years. The broken blue line in **Figure 18** is the second time differential of the R_B/R_{SUN} variation in **Figure 7** and represents, therefore, the acceleration of the Sun along the Sun-barycentre direction. The acceleration indicated by the level 0.001 in **Figure 18** is equivalent to an acceleration of 0.7×10^{-9} m/s^2. This is a small acceleration, about the same as the tidal acceleration on the Sun due to Jupiter [72]; however, it acts over a long time.

For example, the amplitude of the strong positive and negative acceleration peaks indicated in **Figure 18** exceed the level 0.001 for about 20 years. The pink full line is the absolute value of the acceleration and the line with black symbols is a forty year running average over this absolute value. The peaks of the latter
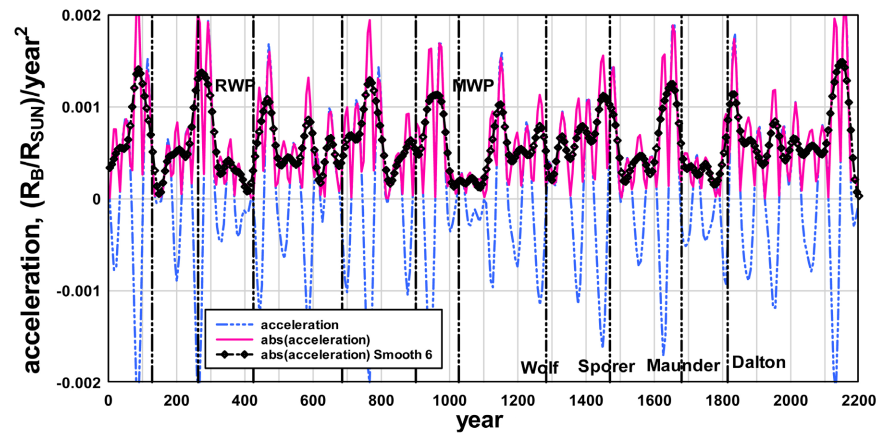
Figure 18. The broken blue curve is the acceleration of the Sun along the Sun-barycentre direction due to planet motion including Planet 9. This curve is the second time differential of the variation of R_B/R_{SUN} with $L_9 = 60°$ in **Figure 7**. The full line pink curve is the absolute value of the acceleration and the black curve with symbols is a 40 year running average over the absolute value. The reference lines mark the centre times of grand solar minima based on the data of Usoskin *et al.* [44] and Inceoglu *et al.* [53]. The intervals associated with the Medieval Warm Period and the Roman Warm Period are also indicated illustrating that these intervals were associated with broad intervals of low Sun acceleration. The 0.001 level in the figure is equivalent to a Sun acceleration of 0.7×10^{-9} m/s^2.

curve correspond to times of strong positive or negative Sun acceleration. The dotted vertical reference lines indicate the centre times of grand solar minima in SSN as estimated from cosmogenic series [44] [53]. The noticeable feature is that times of the centres of grand minima in SSN coincide with the extremes of negative or positive solar inertial acceleration. Thus the inclusion of Planet 9 provides for significant and long acting accelerations of the Sun along the line between the Sun and barycentre and the intervals of stronger acceleration occur within the time intervals encompassing grand solar minima in SSN. It should be noted that similar curves as those shown in **Figure 18** also result from the second time differential of R_B/R_{SUN} when $m_9 = 0$. However, the amplitude of the curves is about tens smaller than when $m_9 = 7 m_E$ indicating that Planet 9 acts to amplify the variation of acceleration.

The variation in **Figure 18** suggests the following mechanism to explain how SIM influences the decrease in solar dynamo action and SSN during grand solar minima. The Sun has a spherical solid core extending to a radius of $0.7 R_{SUN}$ that is separated from a spherical fluid convective outer layer $0.3 R_{SUN}$ thick containing about 2% of the Sun's mass. This is the region where meridional and differentially rotating flows of material occur. When the Sun is accelerating along the line connecting the Sun to the barycentre the fluid convective region is displaced relative to the inner solid core and the convective region bulges in the acceleration direction and thins in the two orthogonal directions. More specifically, because the planets move in the ecliptic plane the convective region thins in the directions perpendicular to the ecliptic plane, in the polar directions. Therefore the result of positive or negative solar acceleration is a thinning of the convective

region at both poles. Simple hydraulic considerations indicate that the meridional and differential rotation flows would be slower in regions where the convective layer is thinner and as a result magnetic activity and sunspot emergence would decrease. In support of this idea, we note that the impedance to hydraulic flow between two parallel planes varies approximately as $1/d^3$ where d is the distance between the planes, the meridional flow converges at the poles reducing the flow cross section, and the thinner convective region near the poles has to accommodate meridional flows both towards and away from the poles; all suggesting strong dependence of meridional flow on the thickness of the convective layer at the poles. Simulation of solar magnetic fields during the Maunder Minimum [29] [73] [74] [75] [76] indicated that the Schwabe sunspot cycle was extremely sensitive to meridional flow speed. The mechanism proposed here provides simultaneous thinning at both poles so that both northern and southern hemisphere meridional flows would be reduced. This would result in symmetric decrease in SSN in both hemispheres. In contrast, the assumption that internal stochastic processes, which would act independently in each hemisphere, affect the meridional flows leads to a highly asymmetric SSN variation [77] with decreased SSN in one hemisphere and normal SSN in the other hemisphere the more likely outcome in this case. Direct measurement of meridional flow on the Sun has been possible only since 1996 with the recent studies [78] [79] finding that a broad reduction in meridional flow speed of about 5 m/s occurred around the year 2000. This direct observation of meridional flow speed reduction corresponds with the weak peak of Sun-barycentre acceleration around year 2000 in **Figure 18** and provides evidence supporting the relationship proposed for the mechanism. We note from **Figure 18** that moderate SIM accelerations are expected to occur ~year 2050 and ~year 2090. However, an interval of extreme Sun acceleration, equivalent to that associated with the Maunder minimum, will not occur until ~year 2130.

The problem faced when proposing the type of mechanism outlined above, and for most mechanisms based on planetary influence on the Sun, is showing that the planetary accelerations are sufficient to cause solar flows large enough to affect the solar dynamo. For example, it is known that by simulating a large variation of meridional flow in the convective layer, it is possible to generate a grand minimum type variation of the solar dynamo [29] [74] [80]. However, the required reduction in meridional flow was found to be about 5 m/s. Whether accelerations of the Sun the order 10^{-9} m/s^2 acting over ~20 years can produce that magnitude of change in the meridional flow is outside the scope of this paper. However, the model outlined above is a mechanism of planet to Sun influence that qualitatively explains many of the observations associated with grand solar minima. Some examples are discussed below.

One example is the occurrence of a normal solar cycle near the middle of solar grand minima. As indicated in **Figure 18** the observed centre times of grand solar minima occur near the times of extreme positive or negative inertial acceleration and the time interval between the acceleration extremes is commensurate

with the duration of grand solar minima, ~50 years, [53]. At the changeover between positive and negative acceleration the solar acceleration is close to zero and meridional flows and the solar dynamo should return to normal function during these short, approximately decade long, intervals. Thus a cycle of near normal amplitude and length would be expected to occur around the middle of grand solar minima. The analysis of reconstructed SSN over the last millennium [45], shows a single, relatively strong, cycle occurs near the middle of the Wolf, Sporer and Maunder grand minima, with the cycle maximum occurring at years 1313, 1494, and 1682. Close examination of Figure 18 shows that the mentioned times coincide with times when solar acceleration is close to zero.

A second example is the provision of a mechanism by which the ~170 year Jose cycle in SIM is phase modulated in the transformation of SIM into SSN. An explanatory mechanism is important as the ~170 year cycle is very prominent in SIM spectra yet is weak, absent, or as discussed above "hidden", in the spectra of SSN and cosmogenic records as reported, for example, by [32] [55]. McCracken *et al.* [32] discussed this issue and concluded that the non-appearance of the ~170 year periodicity in SSN spectra is "*a consequence of the cycle to cycle variability of the Jose cycle as a consequence of the non-commensurate nature of the periods of the Jovian planets*". However, this is a general statement of the problem and not an explanation of it. The mechanism outlined above can explain how the Jose cycle in SIM results in a phase modulated variation in SSN. The basis of a phase modulation mechanism is that an event in solar activity, e.g. the occurrence of a solar grand minimum, should sometimes occur during a positive phase of the Jose cycle in SIM and at other times occur during the negative phase of the Jose cycle in SIM. The Jose cycle in SIM for the last millennium is illustrated in Figure 7. Here we see that the occurrence of grand minima in SSN occur close to sharp turning points in SIM during the negative phase of the Jose cycle. The sharp turning points in R_B/R_{SUN} correspond to times of extreme solar acceleration, and, on the basis of the proposed mechanism, to a reduction in the solar dynamo. Now turning to Figure 10(a) and the variation of SIM in the interval between −7000 to 3000 we notice that, during the interval 0 to 3000, SIM is characterised by sharp negative excursions during the negative phase of the Jose cycle and similarly from −7000 to −5000. However, during the interval −5000 to 0 the SIM is characterised by sharp positive excursions during the positive phase of the Jose cycle. In the mechanism proposed here grand solar minima occur near the times of extreme solar acceleration due to thinning of the convective layer. It follows that during the interval −5000 to 0 grand minima in SSN will occur, predominantly, during the positive phase of the Jose cycle in SIM, whereas, during the intervals −7000 to −5000 and 0 to 3000 grand minima in SSN will occur, predominantly, during the negative phase of the Jose cycle in SIM. As the latter two intervals encompass ~5000 years, and the interval −5000 to 0 also encompasses ~5000 years, we would expect approximately equal occurrence of grand minima in SSN during the positive and during the negative phases of the Jose cycle in SIM. This would result in the appearance of phase

modulation of grand minima in SSN with the centre period of the modulation at the period of the Jose cycle in SIM. Thus, the proposed mechanism resolves the conundrum of the strong Jose component in SIM being an absent or a "hidden" component in SSN as outlined in section 6 of this paper. Occasionally moderately sharp turning points in SIM and accompanying moderately strong accelerations of SIM will occur during the broader intervals in the variation in SIM. For example, the moderately sharp turning points within broad intervals that occur near year 1400 and near year 1910 in Figure 7, would correspond to moderately strong solar acceleration and also result in reductions in SSN. These moderate solar minima, occurring at half intervals of the Jose cycle, would also lead to phase modulation in SSN for similar reasons as discussed above.

While the mechanism described above is mainly qualitative it has, as it is based on planet motion, a predictive capacity. For example, Figure 7, Figure 15 and Figure 18 relate the ~170 year variation in SIM quite accurately to the times of occurrence of the grand minima of SSN in the cluster of grand minima occurring in the last millennium. Further, the occurrence of the cluster can be accurately related to the SIM estimate of the time of occurrence of the minimum of the ~2400 year Hallstatt cycle during the last millennium, at ~year 1500, Figure 10. However, it is clear that the occurrence of solar grand minima is not only due to modulation of the Jose cycle by the Hallstatt cycle but also to the modulation of the Jose cycle by several other low frequency cycles, c.f. Figure 11, Figure 13 and Figure 14. Thus, predicting the occurrence of future grand minima would require knowledge of the phases of the other low frequency cycles as well as the phase of the Hallstaat cycle. It is useful to note that, for dynamo theory based entirely on stochastic simulation of meridional flows, [18] [29] [73] [74] [81], while it is possible to simulate grand solar minima, it is not possible to make predictions of when grand solar minima in SSN will occur. As Wang and Sheeley [73] note, "*the origin of the assumed fluctuations is unknown to us*" and as Karak [74] noted, "*We have no idea why the meridional circulation dropped to a very low value. … However, this assumption enables us to reproduce most of the important features of the Maunder minimum remarkably well*", and as Charbonneau [18] stated "*At this writing we still do not know what triggers Grand Minima, or which physical processes control their duration and drive recovery to 'normal' cyclic activity*".

8. Conclusions

The main hypothesis of this work is that including Planet 9 in the solar system improves the coherence between SIM and SSN. This hypothesis was supported by the demonstration that the important cycles in SSN, the ~2400 year Hallstatt, the ~88 year Gleissberg, the ~60 year, and the 30 year cycles, emerged strongly in SIM when Planet 9 was included in the calculation of SIM. This increase in spectral content with Planet 9 included, c.f. Figure 9(a) and Figure 9(b), is important as it has been suggested, [82], that identifying the principal periodicities observed in solar and climate variability is one of the two crucial tests of whether

there is a planetary influence on the solar dynamo and the variation in solar activity.

The possibility of prediction is an essential feature of the planetary hypothesis. Extrapolating the results obtained in this paper into the future provides the following tentative predictions: The extrapolation of the variation of R_B/R_{SUN} in Figure 1(b) to 2060, indicates that the next three Schwabe cycles will peak in years 2026.8, 2038.5, and 2050.4. Extrapolating Figure 7 and Figure 18 forward to 2200 indicates the next grand solar minimum will be centred on year 2140 and will be very strong, exceeding the strength of the Maunder Minimum. Extrapolating Figure 10(a) forward by several thousand years indicates the next minimum of the Hallstaat cycle will occur at around year 4000.

Conflicts of Interest

The author declares no conflicts of interest regarding the publication of this paper.

References

[1] Brown, M.E. and Batygin, K. (2021) The Orbit of Planet Nine. *The Astronomical Journal*, **162**, Article No. 219. https://doi.org/10.3847/1538-3881/ac2056

[2] Napier, K.J., Gerdes, D.W., Lin, H.W., Hamilton, S.J., Bernstein, G.M., *et al.* (2021) No Evidence for Orbital Clustering in the Extreme Trans-Neptunian Objects. *The Planetary Science Journal*, **2**, Article No. 59.

[3] Holman, M.J. and Payne, M.J. (2016) Observational Constraints on Planet Nine: Astrometry of Pluto and Other Trans-Neptunian Objects. *The Astronomical Journal*, **152**, Article No. 80. https://doi.org/10.3847/0004-6256/152/4/80

[4] Naess, S., Aiola, S., Battaglia, N., Bond, R.J., Calabrese, E., Bond, R.J., Calabrese, E., Choi, S.K., *et al.* (2021) The Atacama Cosmology Telescope: A Search for Planet 9. *The Astronomical Journal*, **923**, Article No. 224. https://doi.org/10.3847/1538-4357/ac2307

[5] Charbonneau, P. (2010) The Planetary Hypothesis Revived. *Nature*, **493**, 613-614. https://doi.org/10.1038/493613a

[6] Jose, P.D. (1965) Suns's Motion and Sunspots. *Astronomical Journal*, **10**, 193-200. https://doi.org/10.1086/109714

[7] Fairbridge, R.W. and Shirley, J.H. (1987) Prolonged Minima and the 179-yr Cycle of the SIM. *Solar Physics*, **110**, 191-220. https://doi.org/10.1007/BF00148211

[8] Charvatova, I. (2000) Can the Origin of the 2400-Year Cycle of Solar Activity Be Caused by SIM. *Annals of Geophysics*, **18**, 399-405. https://doi.org/10.1007/s00585-000-0399-x

[9] Abreu, J.A., Beer, J., Ferriz-Mas, A., McCracken, K.G. and Steinhilber, F. (2012) Is There a Planetary Influence on Solar Activity? *Astronomy & Astrophysics*, **548**, Article No. A88. https://doi.org/10.1051/0004-6361/201219997

[10] Scafetta, N. (2012) Does the Sun Work as a Nuclear Fusion Amplifier of Planetary Tidal Forcing? A Proposal for a Physical Mechanism Based on Mass-Luminosity Relation. *Journal of Atmospheric and Solar-Terrestrial Physics*, **81-82**, 27-40. https://doi.org/10.1016/j.jastp.2012.04.002

[11] Scafetta, N. and Willson, R.C. (2013) Empirical Evidences for a Planetary Modula-

tion of Total Solar Irradiance and the TSI Signature of the 1.09-Year Earth-Jupiter Conjunction Cycle. *Astrophysics and Space Science*, **348**, 25-39. https://doi.org/10.1007/s10509-013-1558-3

[12] Wilson, I.R.G. (2013) The Venus-Earth-Jupiter Spin Orbit Coupling Model. *Pattern Recognition in Physics*, **1**, 147-158. https://doi.org/10.5194/prp-1-147-2013

[13] Scafetta, N., Milani, F., Bianchini, A. and Ortalani, S. (2016) On the Astronomical Origin of the Hallstaat Oscillation in Radiocarbon and Climate Records Throughout the Holocene. *Earth-Science Reviews*, **162**, 24-43. https://doi.org/10.1016/j.earscirev.2016.09.004

[14] Charvatova, I. (2009) Long Term Predictive Assessments of Solar and Geomagnetic Activities Made on the Basis of the Close Similarity Between the Solar Inertial Motions in the Intervals 1840-1905 and 1980-2045. *New Astronomy*, **14**, 25-30. https://doi.org/10.1016/j.newast.2008.04.005

[15] Cionco, R.G. and Soon, W. (2015) A Phenomenological Study of the Timing of Solar Activity Minima of the Last Millennium through a Physical Modeling of the Sun-Planets Interaction. *New Astronomy*, **14**, 164-171. https://doi.org/10.1016/j.newast.2014.07.001

[16] Stefani, F., Giesecke, A., Seilmayer, M., Stepanov, R. and Weir, T. (2020) Schwabe, Gleissberg, Suess-De Vries: Towards a Consistent Model of Planetary Synchronization of Solar Cycles. *Magnetohydrodynamics*, **56**, 269-280. https://doi.org/10.22364/mhd.56.2-3.18

[17] Usoskin, I.G., Sokoloff, D. and Moss, D. (2009) Grand Minima of Solar Activity and the Mean-Field Dynamo. *Solar Physics*, **254**, 345-355. https://doi.org/10.1007/s11207-008-9293-6

[18] Charbonneau, P. (2020) Dynamo Models of the Solar Cycle. *Living Reviews in Solar Physics*, **17**, Article No. 4. https://doi.org/10.1007/s41116-020-00025-6

[19] Tan, B. and Cheng, Z. (2012) Themid-Term and Long-Term Solar Quasi-Periodic Cycles and the Possible Relationship to Planetary Motions. *Astrophysics and Space Science*, **343**, 511-521. https://doi.org/10.1007/s10509-012-1272-6

[20] Eddy, J.A. (1976) The Maunder Mimimum. *Science*, **192**, 1189-1202. https://doi.org/10.1126/science.192.4245.1189

[21] Steinhilber, F., Abreu, J.A., Beer, J., Brunner, I., Christl, M., Fischer, H., *et al.* (2012) 9,400 Years of Cosmic Radiation and Solar Activity from Ice Cores and Tree Rings. *Proceedings of the National Academy of Sciences of the United States of America*, **109**, 5967-5971. https://doi.org/10.1073/pnas.1118965109

[22] Usoskin, I.G., Gallet, Y., Lopes, F., Kovaltsov, G.A. and Hulot, G. (2016) Solar Activity during the Holocene: The Hallstatt Cycle and Its Consequence for Grand Minima and Maxima. *Astronomy & Astrophysics*, **587**, Article No. A150. https://doi.org/10.1051/0004-6361/201527295

[23] Dikpaki, M. and Gilman, P.A. (2006) Simulating and Predicting Solar Cycles Using a Flux-Transport Dynamo. *The Astrophysical Journal*, **649**, 498-514. https://doi.org/10.1086/506314

[24] Zaqarashvili, T.V., Carbonell, M., Oliver, R. and Ballester, J.L. (2010) Quasi-Biennial Oscillations in the Solar Tacholine Caused by Magnetic Rossby Wave Instabilities. *The Astrophysical Journal Letters*, **724**, L95-L98. https://doi.org/10.1088/2041-8205/724/1/L95

[25] Tobias, S., Hughes, D. and Weiss, N. (2006) Unpredictable Sun Leaves Researchers in the Dark. *Nature*, **442**, 26. https://doi.org/10.1038/442026c

[26] Weiss, N.O. and Tobias, S.M. (2016) Supermodulation of the Sun's Magnetic Activ-

ity: The Effects of Symmetry Changes. *Monthly Notices of the Royal Astronomical Society*, **456**, 2654-2661. https://doi.org/10.1093/mnras/stv2769

[27] Beer, J., Tobias, S.M. and Weiss, N.O. (2018) On the Long Term Modulation of the Sun's Magnetic Cycle. *Monthly Notices of the Royal Astronomical Society*, **473**, 1596-1602. https://doi.org/10.1093/mnras/stx2337

[28] Liang, Z.-C., Gizon, L., Birch, A.C. and Thomas, L.D. (2019) Time-Distance Helioseismology of Solar Rossby Waves. *Astronomy & Astrophysics*, **626**, Article No. A3. https://doi.org/10.1051/0004-6361/201834849

[29] Karak, B.B. and Choudhuri, A.R. (2013) Studies of Grand Minima in Sunspot Cycles by Using a Flux Transport Solar Dynamo Model. *Research in Astronomy and Astrophysics*, **13**, 1339-1357. https://doi.org/10.1088/1674-4527/13/11/005

[30] Wolff, C.L. and Patrone, P.N. (2010) A New Way that Planets Can Affect the Sun. *Solar Physics*, **266**, 227-246. https://doi.org/10.1007/s11207-010-9628-y

[31] Landscheidt, T. (1999) Extrema in Sunspot Cycle Linked to Sun's Motion. *Solar Physics*, **189**, 413-424. https://doi.org/10.1023/A:1005287705442

[32] McCracken, K.G., Beer, J. and Steinhilber, F. (2014) Evidence for Planetary Forcing of the Cosmic Ray Intensity and Solar Activity Throughout the Past 9400 Years. *Solar Physics*, **289**, 3207-3229. https://doi.org/10.1007/s11207-014-0510-1

[33] Charvatova, I. (2009) Long-Term Predictive Assessments of Solar and Geomagnetic Activities Made on the Basis of the Close Similarity Between the Solar Inertial Motions in the Intervals 1840-1905 and 1980-2045. *New Astronomy*, **14**, 25-30. https://doi.org/10.1016/j.newast.2008.04.005

[34] Cionco, R.G. and Pavlov, D.A. (2018) Solar Barycentric Dynamics from a New Solar-Planetary Ephemeris. *Astronomy & Astrophysics*, **615**, Article No. A153. https://doi.org/10.1051/0004-6361/201732349

[35] Charvatova, I. and Hejda, P. (2014) Responses of the Basic Cycles of 178.7 and 2402 Yr in Solar Terrestrial Phenomena during the Holocene. *Pattern Recognition in Physics*, **2**, 21-26. https://doi.org/10.5194/prp-2-21-2014

[36] Brown, M.E., Trujillo, C. and Rabinowitz, D. (2004) Discovery of a Planetary-Sized Object in the Scattered Kuiper Belt. *The Astrophysical Journal*, **617**, 645-649. https://doi.org/10.1086/422095

[37] Trujillo, C.A. and Sheppard, S.S. (2014) A Sedna-Like Body with a Perihelion of 80 Astronomical Units. *Nature*, **507**, 471-474. https://doi.org/10.1038/nature13156

[38] Batygin, K. (2016) Pathway to Planet Nine. *Physics World*, **29**, 28-31. https://doi.org/10.1088/2058-7058/29/7/33

[39] Bailey, E., Batygin, K. and Brown, M.E. (2016) Solar Obliquity Induced by Planet Nine. *The Astronomical Journal*, **152**, Article No. 126. https://doi.org/10.3847/0004-6256/152/5/126

[40] Batygin, K., Adams, F.C., Brown, M.E. and Becker, J.C. (2019) The Planet Nine Hypothesis. *Physics Reports*, **805**, 1-53. https://doi.org/10.1016/j.physrep.2019.01.009

[41] Svalgaard, L. and Schatten, K.H. (2016) Reconstruction of the Sunspot Group Number: The Backbone Method. *Solar Physics*, **291**, 2653-2684. https://doi.org/10.1007/s11207-015-0815-8

[42] Perryman, M.A.C. and Schulze-Hartung, T. (2018) The Barycentric Motion of Exoplanet Host Stars. Tests of Solar Spin-Orbit Coupling. *Astronomy & Astrophysics*, **525**, Article No. A65. https://doi.org/10.1051/0004-6361/201015668

[43] Stefani, F., Beer, J., Giesecke, A., Gloaguen, T., Sellmeyer, M., Stepanov, R. and

Weier, T. (2020A) Phase Coherence and Phase Jumps in the Schwabe Cycle. *Astronomische Nachrichten*, **341**, 600-615.

[44] Usoskin, I.G., Solanki, S.K. and Kovaltsov, G.A. (2007) Grand Minima and Maxima of Solar Activity: New Observational Constraints. *Astronomy & Astrophysics*, **471**, 301-309. https://doi.org/10.1051/0004-6361:20077704

[45] Usoskin, I.G., Solanki, S.K., Krivova, N.A., Hofer, B., Kovalstov, G.A., Wacker, L. *et al.* (2021) Solar Activity Over the Last Millennium Reconstructed from Annual 15C Data. *Astronomy & Astrophysics*, **649**, Article No. A141. https://doi.org/10.1051/0004-6361/202140711

[46] Duhau, S. and De Jager, C. (2010) The Forthcoming Grand Minimum of Solar Activity. *Journal of Cosmology*, **8**, 1983-1999.

[47] Feynman, J. and Ruzmaikin, A. (2014) The Centennial Gleissberg Cycle and Its Association with Extended Minima. *Journal of Geophysical Research*: *Space Physics*, **119**, 6027-6041. https://doi.org/10.1002/2013JA019478

[48] Shepherd, S.J., Zharkova, S.I. and Zharkova, V.V. (2014) Prediction of Solar Activity from Solar Background Magnetic Field Variations in Cycles 21-23. *The Astrophysical Journal*, **795**, 46-54. https://doi.org/10.1088/0004-637X/795/1/46

[49] Morner, N.-A. (2015) The Approaching New Grand Solar Minimum and Little Ice Age Climate Conditions. *Natural Science*, **7**, 510-518. https://doi.org/10.4236/ns.2015.711052

[50] Zharkova, V. (2020) Modern Grand Solar Minimum Will Lead to Terrestrial Cooling. *Temperature*, **7**, 217-222. https://doi.org/10.1080/23328940.2020.1796243

[51] Rahmanifard, F., Jordan, A.P., De Wet, W.C., Schwadron, N.A., Wilson, J.K., Owens, M.J., *et al.* (2022) Evidence from Galactic Cosmic Rays That the Sun Has Likely Entered a Secular Minimum in Solar Activity. *Space Weather*, **20**, Article ID: E2021SW002796. https://doi.org/10.1029/2021SW002796

[52] Vasiliev, S.S. and Dergachev, V.A. (2002) The 2400-Year Cycle in Atmospheric Radiocarbon Concentration: Bispectrum of ^{14}C Data Over the Last 8000 Years. *Annals of Geophysics*, **20**, 115-120. https://doi.org/10.5194/angeo-20-115-2002

[53] Inceoglu, F., Simoniello, R., Knudsen, M.F., Karoff, C., Olsen, J, Turek-Chieze, S. and Jacobsen, B.H. (2015) Grand Solar Minima and Maxima Deduced from ^{10}Be and ^{14}C: Magnetic Dynamo Configuration and Polarity Reversal. *Astronomy & Astrophysics*, **577**, Article No. A20. https://doi.org/10.1051/0004-6361/201424212

[54] Vecchio, A., F. Lepreti, F., Laurenza, M., Alberti, T. and Carbone, V. (2017) Connection between Solar Activity Cycles and Grand Minima Generation. *Astronomy & Astrophysics*, **599**, Article No. A58. https://doi.org/10.1051/0004-6361/201629758

[55] Viaggi, P. (2021) Quantitative Impact of Astronomical and Sun-Related Cycles on the Pleistocene Climate System from Antarctica Records. *Quaternary Science Advances*, **4**, Article ID: 100037. https://doi.org/10.1016/j.qsa.2021.100037

[56] Wu, C.-J., Usoskin, I. G, Krivova, N.A., Kovaltsov, G.A., Baroni, M., Bard E., Solanki, S.K. (2018) Solar Activity Over Nine Millennia: A Consistent Multi-Proxy Reconstruction. *Astronomy & Astrophysics*, **615**, Article No. A93. https://doi.org/10.1051/0004-6361/201731892

[57] Scafetta, N. (2010) Empirical Evidence for a Celestial Origin of the Climate Oscillations and Its Implications. *Journal of Atmospheric and Solar-Terrestrial Physics*, **72**, 951-970. https://doi.org/10.1016/j.jastp.2010.04.015

[58] Perez-Peraza, J., Velasco, V., Libin, I.Y. and Yudakhin, K.E. (2012) Thirty Year Pe-

riodicity in Cosmic Rays. *Advances in Astronomy*, **2012**, Article ID: 691408. https://doi.org/10.1155/2012/691408

[59] Damon, P.E. and Peristykh, A.N. (2000) Radiocarbon Calibration and Application of Geophysics, Solar Physics, and Astrophysics. *Radiocarbon*, **42**, 137-150. https://doi.org/10.1017/S0033822200053108

[60] Peristykh, A.N. and Damon, P.E. (2003) Persistence of the Gleissberg 88-Year Cycle over the Last 12,000 Years: Evidence from Cosmogenic Isotopes. *Journal of Geophysical Research*, **108**, 1003-1018. https://doi.org/10.1029/2002JA009390

[61] Takalo, J. and Mursula, K. (2002) Annual and Solar Rotation Periodicities in IMF Components: Evidence for Phase/Freqyency Modulation. *Geophysical Research Letters*, **29**, 1317-1321. https://doi.org/10.1029/2002GL014658

[62] Rial, J.A. (2004) Earth's Orbital Eccentricity and the Rhythm of the Pleistocene Ice Ages: The Concealed Pacemaker. *Global and Planetary Change*, **41**, 81-93. https://doi.org/10.1016/j.gloplacha.2003.10.003

[63] Knudsen, M.F., Riisager, P., Jacobsen, B.H., Muscheler, R., Snowball, I. and Seidenkrantz, M.-S. (2009) Taking the Pulse of the Sun during the Holocene by Joint Analysis of ^{14}C and ^{10}Be. *Geophysical Research Letters*, **36**, Article No. L16701. https://doi.org/10.1029/2009GL039439

[64] Inceoglu, F., Simoniello, R., Knudsen, M.F., Karoff, C., Olsen, J. and Turck-Chièze, S. (2016) On the Current Solar Magnetic Activity in the Light of Its Behaviour during the Holocene. *Solar Physics*, **291**, 303-315. https://doi.org/10.1007/s11207-015-0805-x

[65] Inceoglu, F., Arlt, R. and Rempel, M. (2017) The Nature of Grand Minima and Maxima from Fully Nonlinear Flux Transport Dynamos. *The Astrophysical Journal*, **848**, Article No. 93. https://doi.org/10.3847/1538-4357/aa8d68

[66] Lockwood, M. (2010) Solar Change and Climate: An Update in the Light of the Current Exceptional Solar Minimum. *Proceedings of the Royal Society A*, **466**, 303-329. https://doi.org/10.1098/rspa.2009.0519

[67] Feulner, G. and Rahmsdorf, F. (2010) on the Effect of a New Grand Minimum of Solar Activity on the Future Climate on Earth. *Geophysical Research Letters*, **37**, Article No. L05707. https://doi.org/10.1029/2010GL042710

[68] Meehl, G.A., Arblaster, J.M. and Marsh, D.R. (2013) Could a Future "Grand Solar Minimum" Like the Maunder Minimum Stop Global Warming? *Geophysical Research Letters*, **40**, 1789-1793. https://doi.org/10.1002/grl.50361

[69] Ineson, S., Maycock, A.C., Gray, L.J., Scaife, A.A., Dunstone, N.J., Harder, J.W., *et al.* (2015) Regional Climate Impacts of a Possible Future Grand Solar Minimum. *Nature Communications*, **6**, Article No. 7535. https://doi.org/10.1038/ncomms8535

[70] Velasco Herrera, V.M., Perez-Peraza, J., Soon, W. and Marquez-Adame, J.C. (2018) The Quasi-Biennial Oscillation of 1.7 Years in Ground Level Enhancement Events. *New Astronomy*, **60**, 7-13. https://doi.org/10.1016/j.newast.2017.09.007

[71] Sharp, G.J. (1013) Are Uranus and Neptune Responsible for Solar Grand Minima and Solar Cycle Modulation? *International Journal of Astronomy and Astrophysics*, **3**, 260-273. https://doi.org/10.4236/ijaa.2013.33031

[72] De Jager, C. and Versteegh, G.J.M. (2005) Do Planetary Motions Drive Solar Variability. *Solar Physics*, **229**, 175-179. https://doi.org/10.1007/s11207-005-4086-7

[73] Wang, Y.-M. and Sheeley, N.R. (2003) Modelling the Sun's Large-Scale Magnetic Field during the Maunder Minimum. *The Astrophysical Journal*, **591**, 1248-1256. https://doi.org/10.1086/375449

[74] Karak, B.B. (2010) Importance of Meriodional Circulation in Flux Transport Dynamo: The Possibility of a Maunder-Like Grand Minimum. *The Astrophysical Journal*, **724**, 1021-1029. https://doi.org/10.1088/0004-637X/724/2/1021

[75] Choudhuri, A.R. (2020) The Meridional Circulation of the Sun: Observations, Theory and Connections with the Solar Dynamo. *Science China: Physics, Mechanics and Astronomy*, **64**, Article No. 239601.
https://doi.org/10.1007/s11433-020-1628-1

[76] Miyahara, H., Tokanai, F., Moriya, T., Takeyama, M., *et al.* (2021) Gradual Onset of the Maunder Minimum Revealed by High-Precision Carbon-14 Analyses. *Scientific Reports*, **11**, Article No. 5482. https://doi.org/10.1038/s41598-021-84830-5

[77] Brandenburg, A. and Spiegel, E.A. (2008) Modelling a Maunder Minimum. *Astronomische Nachrichten*, **329**, 351-359. https://doi.org/10.1002/asna.200810973

[78] Hathaway, D.H. and Rightmire, L. (2010) Variations in the Sun's Meridional Flow over a Solar Cycle. *Science*, **327**, 1350. https://doi.org/10.1126/science.1181990

[79] Mahajan, S.S., Hathaway, D.H., Munoz-Jaramillo, A. and Martens, P.C. (2021) Improved Measurements of the Sun's Meridional Flow and Torsional Oscillation from Correlation Trackingon MDI and HMI Magnetograms. *The Astrophysical Journal*, **917**, Article No. 100. Arxiv:2107.07731https://doi.org/10.3847/1538-4357/ac0a80

[80] Passos, D. and Lopes, I. (2008) A Low-Order Solar Dynamo Model: Inferred Meridional Circulation Variations Since 1750. *The Astrophysical Journal*, **686**, 1420-1425. https://doi.org/10.1086/591511

[81] McIntosh, S.W. and Leamon, R.J. (2015) Deciphering Solar Magnetic Activity: On Grand Minima in Solar Activity. *Frontiers in Astronomy and Space Sciences*, **2**, Article No. 2. https://doi.org/10.3389/fspas.2015.00002

[82] Callebaut, D.K., De Jager, C. and Duhau, S. (2012) The Influence of Planetary Attractions on the Solar Tacholine. *Journal of Atmospheric and Solar-Terrestrial Physics*, **80**, 73-78. https://doi.org/10.1016/j.jastp.2012.03.005